Journal of Controlled Release 371 (2024) 455–469

Contents lists available at ScienceDirect

Journal of Controlled Release

journal homepage: www.elsevier.com/locate/jconrel

EGFR-targeted ionizable lipid nanoparticles enhance *in vivo* mRNA delivery to the placenta

Hannah C. Geisler [a], Aditi A. Ghalsasi [a], Hannah C. Safford [a], Kelsey L. Swingle [a], Ajay S. Thatte [a], Alvin J. Mukalel [a], Ningqiang Gong [a], Alex G. Hamilton [a], Emily L. Han [a], Benjamin E. Nachod [a], Marshall S. Padilla [a], Michael J. Mitchell [a,b,c,d,e,f,*]

[a] Department of Bioengineering, University of Pennsylvania, Philadelphia, PA, United States
[b] Penn Institute for RNA Innovation, Perelman School of Medicine, Philadelphia, PA, United States
[c] Abramson Cancer Center, Perelman School of Medicine, University of Pennsylvania, Philadelphia, PA, United States
[d] Institute for Immunology, Perelman School of Medicine, University of Pennsylvania, Philadelphia, PA, United States
[e] Cardiovascular Institute, Perelman School of Medicine, University of Pennsylvania, Philadelphia, PA, United States
[f] Institute for Regenerative Medicine, Perelman School of Medicine, University of Pennsylvania, Philadelphia, PA, United States

ARTICLE INFO

Keywords:
Lipid nanoparticles
Pregnancy
Placenta
Preeclampsia

ABSTRACT

The full potential of ionizable lipid nanoparticles (LNPs) as an *in vivo* nucleic acid delivery platform has not yet been realized given that LNPs primarily accumulate in the liver following systemic administration, limiting their success to liver-centric conditions. The engineering of LNPs with antibody targeting moieties can enable extrahepatic tropism by facilitating site-specific LNP tethering and driving preferential LNP uptake into receptor-expressing cell types *via* receptor-mediated endocytosis. Obstetric conditions stemming from placental dysfunction, such as preeclampsia, are characterized by overexpression of cellular receptors, including the epidermal growth factor receptor (EGFR), making targeted LNP platforms an exciting potential treatment strategy for placental dysfunction during pregnancy. Herein, an EGFR antibody-conjugated LNP (aEGFR-LNP) platform was developed by engineering LNPs with increasing densities of antibody functionalization. aEGFR-LNPs were screened *in vitro* in immortalized placental trophoblasts and *in vivo* in non-pregnant and pregnant mice and compared to non-targeted formulations for extrahepatic, antibody-targeted mRNA LNP delivery to the placenta. Our top performing LNP with an intermediate density of antibody functionalization (1:5 aEGFR-LNP) mediated a ~twofold increase in mRNA delivery in murine placentas and a ~twofold increase in LNP uptake in EGFR-expressing trophoblasts compared to non-targeted counterparts. These results demonstrate the potential of antibody-conjugated LNPs for achieving extrahepatic tropism, and the ability of aEGFR-LNPs in promoting mRNA delivery to EGFR-expressing cell types in the placenta.

1. Introduction

Ionizable lipid nanoparticles (LNPs) have emerged as the most clinically advanced nucleic acid delivery platform following the Food and Drug Administration (FDA) approval of Alnylam's siRNA therapeutic for transthyretin amyloidosis in 2018 and Moderna and Pfizer/BioNTech's COVID-19 mRNA vaccines in 2021 [1–3]. As a non-viral delivery platform, LNPs have demonstrated great preclinical and clinical success given their ability to overcome the *in vivo* barriers to delivery associated with naked nucleic acids, including rapid degradation by nucleases and poor intracellular uptake due to their large size and negative charge [4,5]. Because LNPs are able to efficiently encapsulate large, negatively-charged nucleic acid cargo, systemic administration of LNPs has enabled intracellular uptake and potent protein expression in a variety of cell types [2,6,7].

Despite these key advantages, challenges remain in developing new LNP platforms for broad use across disease applications given that LNPs primarily accumulate in the liver through the first-pass hepatic clearance effect and apolipoprotein E (ApoE)-mediated pathways [8]. As a result, LNPs are rapidly cleared from the bloodstream and have been limited in their application for liver-centric conditions [9–11]. However, recent pre-clinical studies have highlighted the importance of rational

* Corresponding author at: Department of Bioengineering, University of Pennsylvania, 210 S. 33rd St., 240 Skirkanich Hall, Philadelphia, PA 19104, U.S.
E-mail address: mjmitch@seas.upenn.edu (M.J. Mitchell).

https://doi.org/10.1016/j.jconrel.2024.05.036
Received 30 November 2023; Received in revised form 15 May 2024; Accepted 19 May 2024
Available online 10 June 2024

design in the development of novel LNP platforms, which have enabled LNP-mediated mRNA delivery to extrahepatic organs including the spleen, lungs, and bone marrow [12–14] and demonstrated the therapeutic potential of LNP platforms in treating conditions of extrahepatic origin. Together, these works highlight the ongoing need for the inclusion of novel design features to engineer LNP formulations capable of escaping hepatic clearance and achieving extrahepatic, tissue-specific delivery.

Recently, our group and others have begun to investigate the use of mRNA LNPs for therapeutic applications during pregnancy – specifically for extrahepatic mRNA delivery to the placenta to treat placental dysfunction [15–18]. The placenta is a transient organ that develops during pregnancy, wherein it acts to protect the fetus from potentially harmful agents in maternal circulation while mediating nutrient/oxygen exchange [19]. As pregnancy progresses, approximately one-quarter of cardiac output gets shunted to the developing placenta and fetus [20], and maternal utero-placental (spiral) arteries undergo rapid remodeling to support this newfound demand for blood supply [21,22]. Dangerous obstetric complications, including preeclampsia, fetal growth restriction, miscarriage, preterm labor, and fetal death, can arise when dysfunctional placental development and/or vascular remodeling occurs [22,23]. Many conditions that arise from placental dysfunction, including preeclampsia, are marked by systemic under- or over-expression of specific pathologic proteins, making placental disorders an attractive application for LNP-mediated nucleic acid therapy. However, given ethical concerns regarding the potential toxicity of therapeutic agents to the unborn fetus, pregnant patients have been historically excluded from clinical trials, resulting in a substantial shortage of therapeutics approved for obstetric complications [24–27] and presenting a potential need for sophisticated nanoparticle platforms capable of achieving tissue-specific delivery to the placenta while limiting transfer of therapeutic agents from the maternal bloodstream into fetal circulation.

Since LNP shape, size, and chemical composition can influence their biodistribution, preclinical studies have largely focused on modulating physicochemical LNP properties to manipulate *in vivo* fate and achieve extrahepatic delivery [28,29]. Besides altering physicochemical properties, LNP tissue tropism can be achieved through active targeting approaches, including nanoparticle conjugation to chemical or biological moieties such as antibodies, peptides, aptamers, and more [30–33], which possess innate affinity for cellular receptors or membrane proteins [11,29]. The use of active targeting is particularly advantageous in diseased states marked by abundant overexpression of cellular receptors, as targeting moieties can enable site-specific accumulation and tethering of LNPs. Further, active targeting moieties can drive preferential nanoparticle uptake *via* receptor-mediated endocytosis into key cell types implicated in a given disease (Fig. 1A), reducing drug exposure in off-target tissues, and thereby increasing therapeutic efficacy

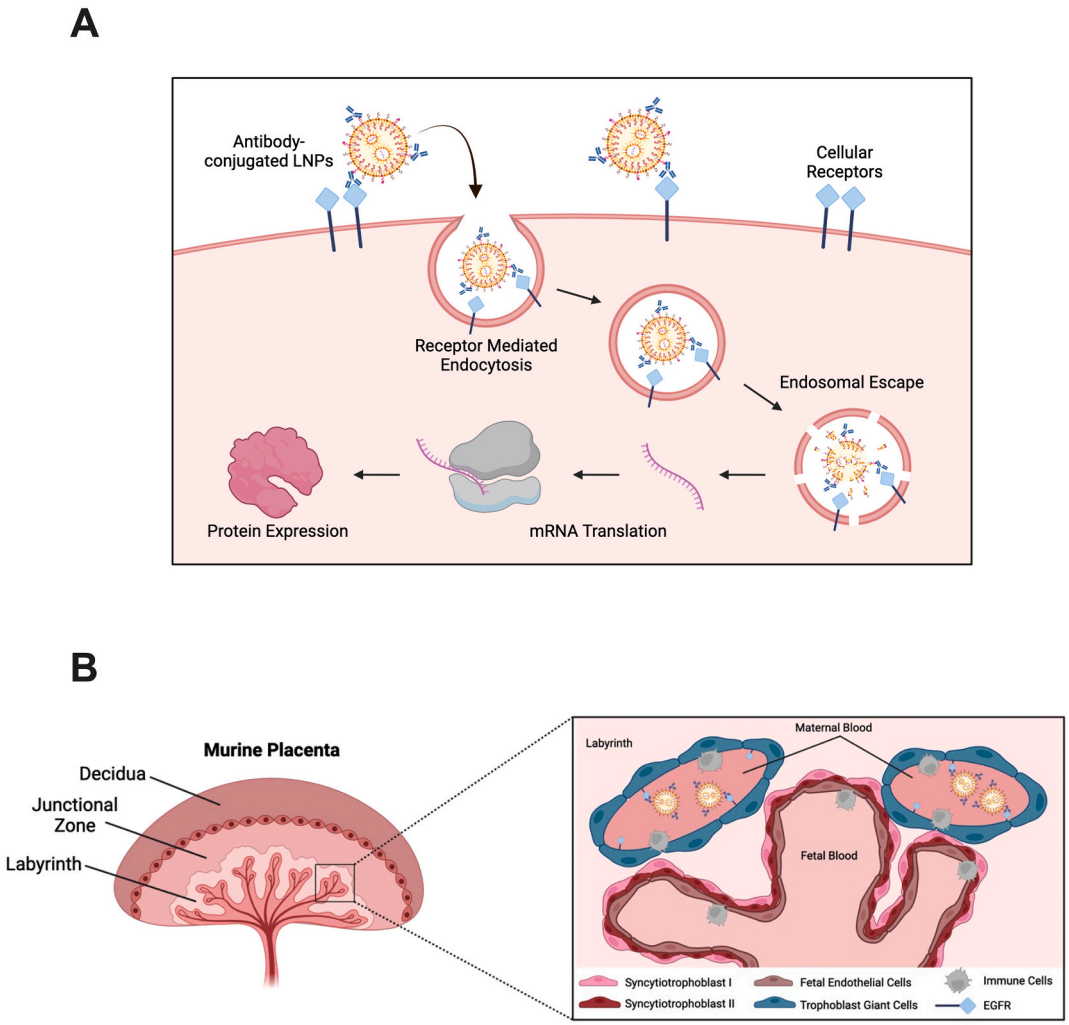

Fig. 1. Antibody-conjugated ionizable lipid nanoparticles (LNPs) for targeted mRNA delivery to the murine placenta. (A) Schematic depicting cellular uptake of antibody-conjugated LNPs in placental cells *via* receptor-mediated endocytosis. **(B)** Left: structure of the murine placenta. Right: zoomed in view of the placental labyrinth where EGFR antibody-conjugated LNPs in maternal blood come in contact with EGFR-expressing trophoblast giant cells in the placenta.

[34]. In addition, it has been reported that actively targeted nanoparticles demonstrate enhanced therapeutic efficacy at lower doses when compared to their passively targeted counterparts, allowing for potential dose sparing and improved safety profiles, which is particularly critical in the design of therapeutics for obstetric conditions [35]. To this end, we sought to engineer LNPs with active targeting moieties to enhance mRNA delivery to the placenta during pregnancy.

In previous works, maleimide-thiol chemistry has frequently been employed to generate ligand-decorated nanoparticles [36–38]; however, maleimide is susceptible to hydrolysis, and studies have shown that preparation methods, including nanoparticle dialysis in PBS, can decrease maleimide reactivity by up to 50% [39,40]. Further, the use of maleimide-thiol chemistry has been reported to produce diverse reaction products [41]. Another popular conjugation strategy, the anchored secondary scFv enabling targeting platform, or ASSET, has demonstrated successful targeting to a variety of cell types [42,43], but requires production of recombinant proteins and is currently limited by antibody isotype [44]. Given these limitations, we chose to employ strain-promoted azide alkyne cycloaddition (SPAAC), known for its highly efficient kinetics and selectivity [45], to engineer antibody-conjugated LNPs. Importantly, SPAAC chemistry can be performed in mild reaction conditions and is insensitive to oxygen and water [46], allowing for simple, straight-forward production of stable antibody-conjugated LNPs.

In this work, we engineered epidermal growth factor receptor (EGFR) antibody-conjugated LNPs (aEGFR-LNPs) to increase trophoblast-specific uptake and mRNA expression in the placenta for applications in treating pregnancy complications. We utilized SPAAC chemistry to engineer LNPs with increasing amounts of EGFR antibody on the LNP surface. Luciferase mRNA expression of aEGFR-LNPs was evaluated *in vitro* in immortalized placental trophoblasts and *in vivo* in non-pregnant and pregnant mice. Our top performing LNP with an intermediate density of antibody functionalization demonstrated enhanced *in vivo* luciferase expression in murine placentas compared to non-targeted formulations. We show that DiR-labeled aEGFR-LNPs exhibit a ~twofold increase in cellular uptake in EGFR-expressing trophoblasts compared to non-targeted counterparts. Together, these results demonstrate the use of antibody-conjugated LNPs for achieving extrahepatic tropism and the ability of aEGFR-LNPs to enhance mRNA delivery to the placenta with the potential to treat obstetric conditions.

2. Results and discussion

2.1. Engineering EGFR antibody-conjugated LNPs

Recent work by our group identified a novel ionizable lipid, C12–494, capable of facilitating mRNA LNP delivery to the placenta [15]. To further enhance placental tropism with this LNP formulation, we sought to functionalize the LNP surface with antibody moieties targeting EGFR. EGFR is abundantly expressed in both human and murine placentas (Fig. 1B) and plays a vital role in regulating growth and development of trophoblasts — the main cell type of the placenta [47,48]. Importantly, EGFR expression is primarily found in trophoblasts that are in direct contact with maternal blood — the syncytiotrophoblast layer [48,49] and trophoblast giant cells [50] in humans and mice, respectively. EGFR expression is further upregulated during placental dysfunction [51], making EGFR an attractive receptor for targeted drug delivery to the placenta during both healthy and dysfunctional pregnancies.

Here, we formulated LNPs with the C12–494 ionizable lipid and conjugated EGFR antibodies to the LNP surface to enable active targeting to the placenta. LNPs were formulated *via* chaotic mixing in a microfluidic device by combining an organic lipid phase and an aqueous mRNA phase as previously described [52]. Lipid components were combined in ethanol according to the standard excipient molar ratios used for mRNA delivery: 35% ionizable lipid, 16% 1,2-dioleoyl-*sn*-glycero-3-phosphoethanolamine (DOPE), 46.5% cholesterol, and 2.5% lipid-anchored polyethylene glycol (PEG) [6]. To facilitate antibody functionalization, lipid-anchored PEG-azide was substituted as a fraction of the total lipid-PEG at varying ratios (**Table S1**), as the addition of azide to the LNP surface allows for conjugation with dibenzocyclooctyne (DBCO)-labeled antibodies *via* SPAAC [40,53].

It is well understood that the density of targeting moieties on the surface of nanoparticles can influence LNP fate, including protein corona formation, LNP biodistribution, and cellular-level LNP uptake [29,54]. More specifically, studies have demonstrated that intermediate ligand densities may be preferred for cellular-level targeting, as high ligand densities can saturate cellular receptors [54,55]. However, the relationship between targeting ligand density and nanoparticle uptake may depend on other factors, such as receptor density in the cellular membrane and receptor spatial orientation [55]. Here, LNPs were generated with four different molar substitution ratios of lipid-PEG-azide:lipid-PEG (1:2, 1:3, 1:5, and 1:7) to evaluate the influence of antibody functionalization density on mRNA LNP delivery to placental trophoblasts. Following microfluidic formulation, azide-containing LNPs were incubated overnight with DBCO-functionalized EGFR antibodies to generate aEGFR-LNPs (Fig. 2A), and unconjugated antibodies were separated from LNPs *via* size exclusion chromatography. Throughout this work, mRNA transfection efficiency of aEGFR-LNPs was compared against two non-targeted formulations: LNP S1, a standard formulation containing no azide, and LNP A1, an azide control formulation containing a 1:5 substitution of lipid-PEG-azide:lipid-PEG.

After formulation, LNPs were characterized on the basis of size, antibody concentration, mRNA encapsulation efficiency, zeta potential, stability, and pK_a.(**Table S1, Table S2**). Successful antibody conjugation to the LNP surface was marked by an increase in LNP size measured using dynamic light scattering (DLS). The addition of lipid-PEG-azide alone (LNP A1) did not change LNP diameter when compared to the standard formulation (LNP S1) and, thus, the observed increases in LNP diameter for aEGFR-LNPs were attributed to antibody conjugation (**Table S2**). LNP size and antibody functionalization density increased monotonically with increasing substitution of lipid-PEG-azide (Fig. 2B, **Table S1**), perhaps owing to the highly efficient kinetics of SPAAC chemistry [40]. The zeta potential of all LNPs remained overall neutral, with the surface charge of aEGFR-LNPs decreasing slightly compared to the non-targeted formulations, consistent with the weak negative net charge carried by immunoglobulins [56]. Antibody conjugation and subsequent size exclusion chromatography did not affect mRNA encapsulation efficiency (Fig. 2C). To examine whether antibody functionalization affects LNP stability over time, LNPs were incubated in PBS at 37 °C for 48 h, and LNP diameter was measured at one-hour intervals *via* DLS. All LNPs remained stable over the 48 h period, with no indications of significant aggregation of aEGFR-LNPs when compared to LNP S1 and LNP A1 (Fig. 2D). LNP pK_a values ranged from 5.7 to 6.6 (Fig. 2E), with the pK_a of aEGFR-LNPs remaining comparable to non-targeted formulations.

2.2. aEGFR-LNPs enhance in vitro mRNA delivery to trophoblasts

To evaluate whether aEGFR-LNPs can enhance *in vitro* mRNA delivery, LNPs were formulated encapsulating nucleoside-modified luciferase mRNA as a reporter cargo. *In vitro* screening was performed in the EGFR-expressing human choriocarcinoma JEG-3 cell line, a common *in vitro* model of human placental trophoblasts [33,57]. JEG-3 cells were treated with LNP S1, LNP A1, or aEGFR-LNPs at a dose of 50 ng of mRNA per 50,000 cells, and luciferase expression as a measure of functional mRNA delivery was evaluated 24 h following treatment (Fig. 3A). Luciferase mRNA delivery with LNP A1 did not differ from luciferase mRNA delivery with the previously validated placenta-tropic S1 LNP formulation, confirming that the addition of lipid-PEG-azide in the LNP formulation alone does not confer active targeting capabilities, nor does the addition of lipid-PEG-azide decrease LNP-mediated *in vitro* luciferase

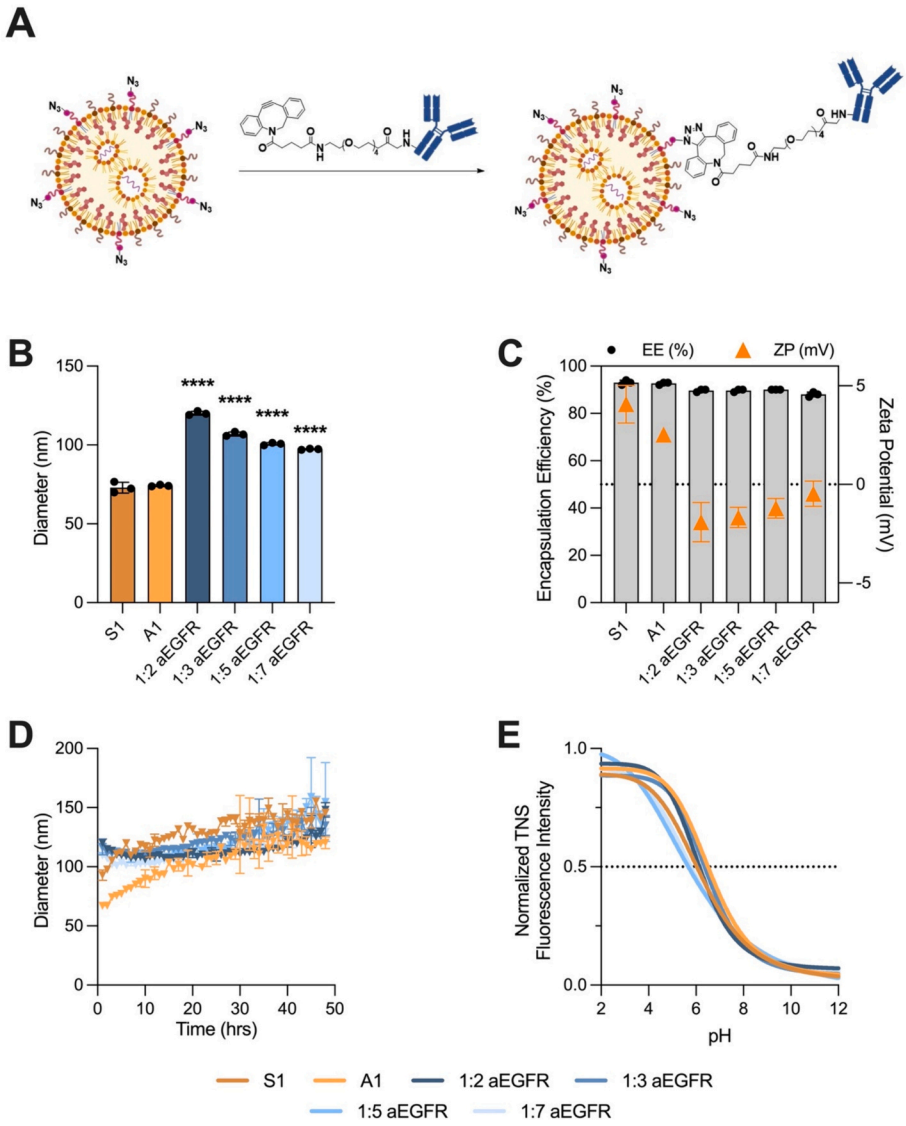

Fig. 2. aEGFR-LNP formulation and characterization. **(A)** LNPs containing lipid-PEG-azide were reacted with DBCO-labeled EGFR antibodies to generate EGFR antibody-conjugated LNPs (aEGFR-LNPs). **(B)** Hydrodynamic (z-average) diameter, **(C)** mRNA encapsulation efficiency, zeta potential, **(D)** hydrodynamic (z-average) diameter in aqueous solution over 48 h, and **(E)** pK_a characterization of non-targeted LNP S1 and LNP A1 and aEGFR-LNPs with decreasing densities of antibody functionalization. Data are reported as mean ± standard deviation (n = 3 observations). Ordinary one-way ANOVA with *post hoc* Student's *t*-tests using the Holm–Šídák correction for multiple comparisons was used to compare hydrodynamic diameter to LNP A1. ****$p \leq 0.0001$.

mRNA delivery. Given this finding, the measured luciferase expression for all aEGFR-LNPs was compared to LNP A1 in all subsequent experiments. Three of the aEGFR-LNP antibody densities (1:2, 1:3, and 1:5 aEGFR-LNPs) demonstrated a significant increase in luciferase mRNA delivery compared to LNP A1. The highest luciferase expression was observed with the highest density of antibody functionalization (1:2 aEGFR-LNPs), with luciferase expression decreasing across lower antibody densities (1:3 and 1:5 aEGFR-LNPs). Luciferase expression following treatment with the lowest density of antibody functionalization (1:7 aEGFR-LNPs) did not significantly differ from LNP S1 and LNP A1 non-targeted controls. To confirm that enhanced luciferase expression following treatment with aEGFR-LNPs was specific to EGFR targeting, 1:5 aEGFR-LNPs were screened *in vitro* against LNPs conjugated with CD3 antibodies (1:5 aCD3-LNPs) as a negative control for placental trophoblasts **(Fig. S1).** EGFR antibody-conjugated LNPs demonstrated enhanced luciferase expression compared to LNP A1, but luciferase expression following treatment with CD3 antibody-conjugated LNPs did not differ significantly from LNP A1, confirming that the presence of antibodies alone is not sufficient to confer enhanced, targeted mRNA delivery to trophoblasts. Finally, cell viability was not affected across formulations at a dose of 50 ng of mRNA per 50,000 cells. (Fig. 3B).

Next, we sought to examine the effects of EGFR antibody-targeting on *in vitro* luciferase expression and cytotoxicity in a dose-dependent manner. At doses ranging from 10 ng – 100 ng of mRNA per 50,000 cells, all four aEGFR-LNPs demonstrated a significant increase in luciferase expression compared to LNP A1 (Fig. 3C). Consistent with our initial screen at a dose of 50 ng of mRNA, the most densely functionalized nanoparticle formulation (1:2 aEGFR-LNPs) induced the highest luciferase expression compared to LNP A1, while the least densely functionalized nanoparticle formulation (1:7 aEGFR-LNPs) mediated the least improvement in luciferase mRNA delivery compared to LNP A1 across most doses. As the mRNA dose increased, enhancement in luciferase expression for all aEGFR-LNPs decreased compared to the non-targeted LNP A1, potentially due to a saturation of EGFR receptors [58]. At the highest dose tested, luciferase expression mediated by aEGFR-LNPs did not significantly differ from LNP A1. To quantify this effect, we examined the fold change in luminescence across doses for aEGFR-LNPs compared to LNP A1 (**Fig. S2**); all aEGFR-LNPs

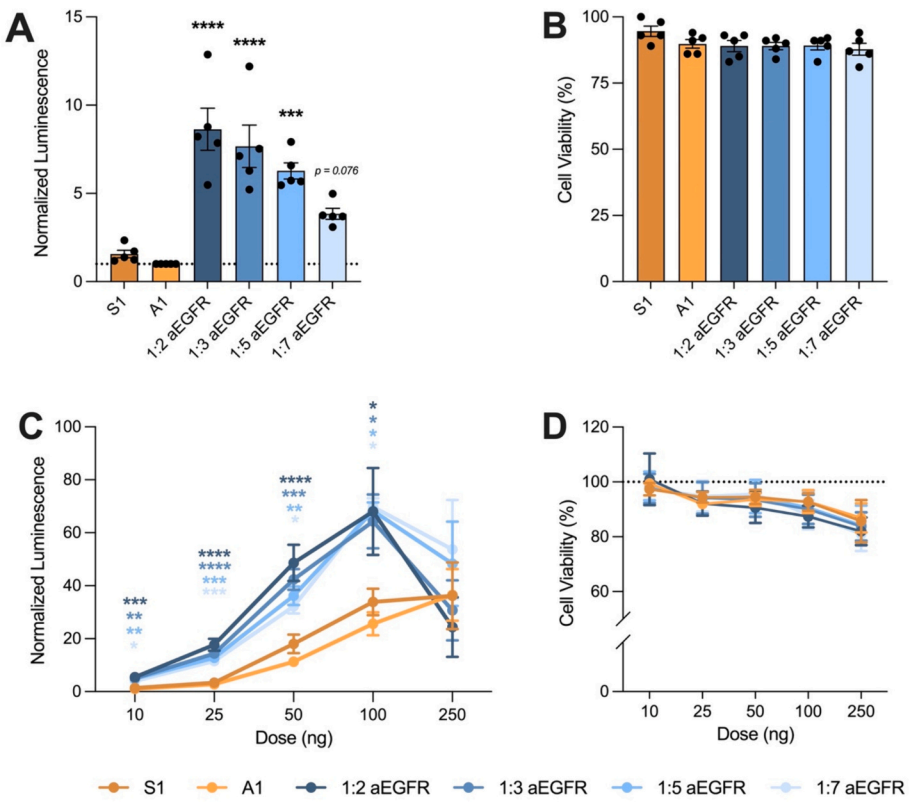

Fig. 3. aEGFR-LNPs enhance luciferase mRNA delivery to placental trophoblasts *in vitro*. **(A)** Luciferase expression and **(B)** cell viability in JEG-3 trophoblast cells 24 h after treatment with non-targeted LNPs S1 or A1 or aEGFR-LNPs at a dose of 50 ng of luciferase mRNA per 50,000 cells. Normalized luciferase expression was quantified by subtracting bioluminescence values from untreated cells and normalizing to cells treated with LNP A1 (dashed line in (**A**)). **(C)** Luciferase expression and **(D)** cell viability in JEG-3 trophoblast cells 24 h after treatment with non-targeted LNPs S1 or A1 or aEGFR-LNPs. Cells were treated in a dose-dependent manner at 10, 25, 50, 100, and 250 ng of luciferase mRNA per 50,000 cells. Normalized luciferase expression was quantified by subtracting bioluminescence values from untreated cells and normalizing to cells treated with LNP A1 at the lowest dose. Percent cell viability for each treatment condition was normalized to untreated cells. Results are reported as mean ± SEM from $n = 5$ biological replicates. Nested one-way ANOVA with *post hoc* Student's *t*-tests using the Holm–Šídák correction for multiple comparisons was used to compare the luciferase expression or cell viability across treatment groups to LNP A1. * $p \leq 0.05$, ** $p \leq 0.01$, ***$p \leq 0.001$, ****$p \leq 0.0001$.

demonstrated the greatest increase in luciferase expression at doses of 10 ng and 25 ng of mRNA, consistent with previous works reporting that therapeutic efficacy requires lower doses of actively targeted nanoparticles compared to their non-targeted counterparts [35]. Importantly, minimal cytotoxicity was observed across formulations when compared to LNP A1 (Fig. 3D).

2.3. Pregnancy alters aEGFR-LNP in vivo biodistribution

Three out of four aEGFR-LNP formulations (1:2, 1:3, and 1:5 aEGFR-LNPs) demonstrated strong and consistent improvements in luciferase mRNA delivery *in vitro* compared to LNP A1 across most doses and, thus, were selected for further screening *in vivo*. Given the current lack of knowledge surrounding changes in nanoparticle behavior due to physiologic changes that occur during pregnancy, we first chose to evaluate biodistribution of aEGFR-LNPs in non-pregnant and pregnant mice. LNPs were formulated encapsulating luciferase mRNA, and non-pregnant and gestational day E16 pregnant mice were treated with PBS, LNP S1, LNP A1, or aEGFR-LNPs at a dose of 0.4 mg of mRNA per kg body mass *via* tail vein injection. 6 h after treatment, mice received an intraperitoneal injection of *D*-luciferin before euthanasia. Maternal organs, placentas, and fetuses were removed for bioluminescence imaging using an *in vivo* imaging system (IVIS).

In our previous work, LNPs formulated with the placenta-tropic C12–494 ionizable lipid demonstrated reduced liver delivery and enhanced splenic delivery compared to an industry standard liver-tropic C12–200 LNP formulation, potentially due to increased electronegativity conferred by the presence of ether bonds in the C12–494 structure [15,16]. As expected, we observed similar tropism with all of our LNP formulations in this work, with substantial extrahepatic luciferase expression in the spleen and low luciferase expression in the liver in both non-pregnant and pregnant mice (Fig. 4A,B). Interestingly, aEGFR-LNPs, but not their non-targeted counterparts, trended towards higher spleen:liver luminescence ratios in pregnant mice compared to non-pregnant mice (**Fig. S3).**

In non-pregnant mice, 1:3 and 1:5 aEGFR-LNPs demonstrated enhanced luciferase expression in the liver and spleen compared to LNP A1 (Fig. 4C) whereas, in pregnant mice, luciferase expression in the liver and spleen following treatment with aEGFR-LNPs did not differ significantly from LNP A1 (Fig. 4D). Only 1:5 aEGFR-LNPs resulted in higher mean luciferase expression ($p = 0.055$) in the spleens of pregnant mice compared to LNP A1. In humans, the placenta is the highest EGFR-expressing organ; however, in mice, abundant EGFR expression has been reported in the placenta and liver [50,59,60]. Thus, the observed enhanced luciferase expression with aEGFR-LNPs in the livers of non-pregnant mice compared to LNP A1 may be a result of targeted delivery to EGFR-expressing cells in the liver. In fact, 1:3 and 1:5 aEGFR-LNPs significantly enhanced luciferase expression in the livers of non-pregnant mice compared to pregnant mice (**Fig. S4**). The reduction in liver delivery of aEGFR-LNPs in pregnant mice compared to non-pregnant mice is likely then a result of shifted cardiac output during pregnancy, combined with active targeting to the EGFR-expressing placentas.

The enhanced splenic delivery of 1:5 aEGFR-LNPs compared to LNP

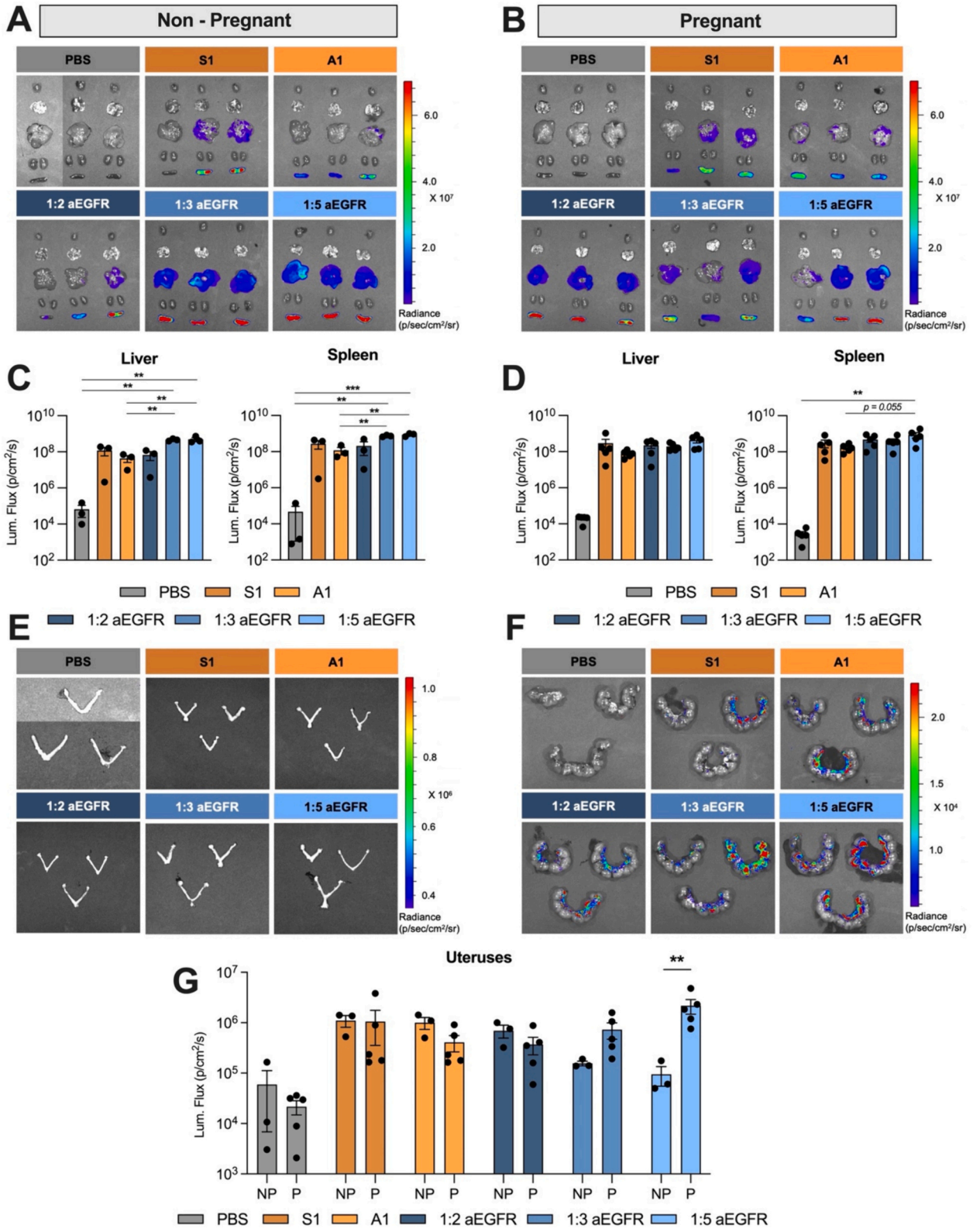

Fig. 4. Pregnancy alters aEGFR-LNP luciferase mRNA delivery to maternal organs *in vivo*. **(A,B)** IVIS images of luciferase mRNA translation in the heart, lungs, liver, kidneys, and spleen in **(A)** non-pregnant and **(B)** pregnant mice following treatment with non-targeted LNPs S1 or A1 or aEGFR-LNPs (0.4 mg mRNA/kg body mass). **(C, D)** Quantification of luciferase mRNA expression in the liver and spleen in **(C)** non-pregnant and **(D)** pregnant mice. Luminescence flux is reported as mean ± SEM from $n = 3$ biological replicates for non-pregnant mice and $n = 5$ biological replicates for pregnant mice. One-way ANOVA with *post hoc* Student's *t*-test using the Holm–Šídák correction for multiple comparisons was used to compare luciferase expression in the liver and spleen across treatment groups to LNP A1. **(E,F)** IVIS images of luciferase mRNA delivery (0.4 mg mRNA/kg body mass) to the uteruses in **(E)** non-pregnant and **(F)** pregnant mice. **(G)** Quantification of luminescence flux in the uteruses of non-pregnant (NP) and pregnant (P) mice. Two-way ANOVA with *post hoc* Student's *t*-tests using the Holm–Šídák correction for multiple comparisons was used to compare luminescence flux in uteruses across LNP treatment groups in NP *vs.* P mice. $^{**}p \leq 0.01$, $^{***}p \leq 0.001$.

A1 in both non-pregnant and pregnant mice is potentially a result of antibody-conjugated LNP trafficking to the spleen. It has been reported that the spleen is a site of accumulation for monoclonal antibodies: increased leakiness of splenic capillary beds demonstrate decreased repulsion and enhanced penetration of negatively charged immunoglobulins [61,62]. Following accumulation in the spleen, antibodies may then be cleared from circulation *via* immune cell-mediated pathways or recycled *via* the neonatal Fc receptor (FcRn). Given their role as phagocytic blood filters, splenic macrophages and neutrophils in the spleen interact with Fc regions on antibodies, leading to internalization and destruction [61]. The spleen also has rich FcRn expression, which may facilitate immunoglobulin recycling to plasma. In fact, it has been reported that the spleen demonstrates the highest catabolic activity compared to all other organs for the clearance of antibodies with FcRn affinity but not for antibodies lacking FcRn affinity [61,63]. Interestingly, splenic luciferase expression with 1:3 and 1:5 aEGFR-LNPs was higher in non-pregnant mice compared to pregnant mice (**Fig. S5**), which may be explained by the decreased alloimmune responses observed during pregnancy due to the presence of the partially allogenic fetus [64]. Together, these results suggest that the engineering of LNPs with monoclonal antibodies can mediate extrahepatic delivery to the spleen. Further, the use of antibody targeting may be advantageous during pregnancy, as reduced alloimmune responses may limit antibody trafficking to the spleen and subsequently enhance targeted delivery to the placenta. These findings highlight the importance of screening therapeutic platforms in pregnancy models, as pregnancy can result in not only organ-level changes in biodistribution but also changes in nanoparticle uptake and clearance.

LNP delivery to the uterus was also evaluated in both non-pregnant and pregnant mice (Fig. 4E,F). Interestingly, in non-pregnant mice, the non-targeted LNP S1 and LNP A1 formulations resulted in the highest uterine luminescence, whereas 1:3 and 1:5 aEGFR-LNPs demonstrated very little uterine delivery. However, increased luminescence was observed in pregnant mice with 1:3 and 1:5 aEGFR-LNPs (**Fig. S6).** These results may be explained by the role of EGFR in the murine uterine stroma, where EGFR signaling regulates uterine development and embryo implantation during pregnancy [65]. 1:5 aEGFR-LNPs resulted in a significant increase in luciferase expression in the uteruses of pregnant mice compared to non-pregnant mice (Fig. 4G), suggesting that an intermediate antibody density may be optimal for EGFR targeting to the uterus during pregnancy.

2.4. aEGFR-LNPs enhance extrahepatic mRNA delivery to the placenta in pregnant mice

Next, we evaluated luciferase mRNA delivery to the placentas and fetuses of pregnant mice to examine the effects of engineered aEGFR-LNPs in promoting active targeting to EGFR-rich placentas (Fig. 5A). Consistent with the observed uterine mRNA LNP delivery in pregnant mice, the 1:5 aEGFR-LNP formulation resulted in a significant increase (~2X) in luciferase expression in placentas compared to LNP A1 and all other LNP treatment groups (Fig. 5B).

In contrast with our *in vitro* findings, aEGFR-LNPs with higher antibody density functionalization (1:2 and 1:3 aEGFR-LNPs) did not result in enhanced *in vivo* luciferase mRNA LNP delivery to the placenta. These results confirm previous reports that *in vitro* screening is not always predictive of *in vivo* nanoparticle behavior [66,67]. These findings suggest that densely functionalized LNPs may perform best *in vitro* given the static nature of cells and widespread availability of receptors; however, intermediate densities of targeting moieties appear to be optimal *in vivo*, potentially due to reduced steric hindrance effects and subsequent availability of antigen binding sites [54]. Given that whole antibodies were used to formulate our aEGFR-LNPs, it is also possible that the increased availability of Fc regions on more densely antibody-conjugated LNPs (1:2 aEGFR-LNPs) increases the likelihood of recognition and phagocytosis by macrophages of the mononuclear phagocyte system (MPS), leading to their rapid clearance [68,69].

In agreement with our previous work, bioluminescence was not detected in fetuses for any LNP-treated groups (Fig. 5C), suggesting that LNPs do not exhibit placental transfer into fetal circulation, likely due to their large size [18]. Together, these results demonstrate the potential of 1:5 aEGFR-LNPs in enhancing extrahepatic, tissue-specific delivery to EGFR-expressing placentas.

2.5. aEGFR-LNPs exhibit comparable splenic immune cell accumulation

Because 1:5 aEGFR-LNPs resulted in higher splenic luminescence compared to LNP A1 in both non-pregnant and pregnant mice during

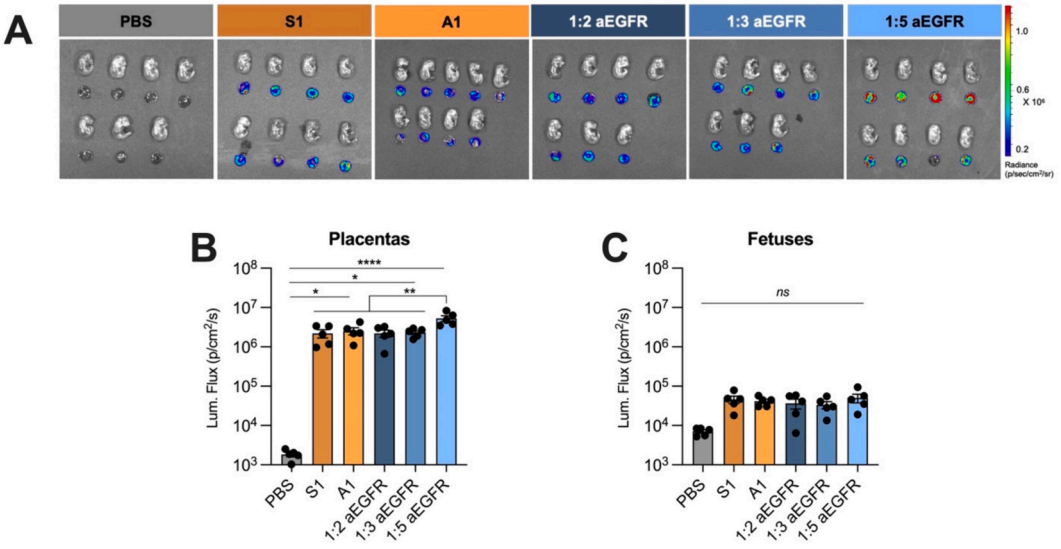

Fig. 5. aEGFR-LNPs increase luciferase mRNA delivery to placentas *in vivo*. (A) IVIS images of luciferase mRNA expression in murine placentas and fetuses following treatment with non-targeted LNPs S1 or A1 or aEGFR-LNPs (0.4 mg mRNA/kg body mass). Quantification of luminescence flux in the **(B)** placentas and **(C)** fetuses in pregnant mice. Luminescence flux is reported as mean ± SEM from $n = 5$ biological replicates with $n = 3$–9 placentas and fetuses per mouse. Nested one-way ANOVA with *post hoc* Student's *t*-tests using the Holm–Šídák correction for multiple comparisons was used to compare flux across treatment groups, $^{*}p \leq 0.05$, $^{**}p \leq 0.01$, $^{***}p \leq 0.001$.

biodistribution experiments, we then evaluated cellular-level uptake of aEGFR-LNPs in murine spleens in pregnant mice to identify potential antibody-mediated immune responses and evaluate potential antibody-mediated influence on LNP accumulation in immune cell types. To this end, LNP A1 and 1:5 aEGFR-LNPs were labeled with the lipophilic fluorescent DiR dye and administered to pregnant mice at a dose of 1 mg of mRNA per kg body mass *via* tail vein injection. 12 h after injection, mice were euthanized and organs were imaged.

DiR fluorescence flux in the spleen was significantly higher with LNP A1 than with 1:5 aEGFR-LNPs (Fig. 6A, **Fig. S11**). Interestingly, higher mean luciferase expression was observed in the spleen during biodistribution experiments ($p = 0.055$) with 1:5 aEGFR-LNPs compared to LNP A1. These results suggest that while 1:5 aEGFR-LNPs may promote potent luciferase mRNA delivery and expression once inside the cell, modification of this spleen-tropic LNP formulation with EGFR antibodies may actually reduce LNP accumulation in the spleen during pregnancy and promote extrahepatic LNP accumulation in the placenta.

To quantify LNP uptake at the cellular level, spleens were processed to generate single cell suspensions and examined for DiR fluorescence *via* flow cytometry. It has been widely established that fluorescent proteins, such as mCherry and GFP, often require multiple copies in order to detect signal *via* flow cytometry [70], and thus are not an ideal model for evaluating mRNA delivery *in vivo*. Given that our biodistribution studies confirmed the ability of aEGFR-LNPs in facilitating functional luciferase mRNA expression, we opted to instead evaluate the DiR fluorescent dye as a metric of LNP uptake in cell types in the spleen to investigate whether the engineering of LNPs with EGFR antibodies influences splenic cellular-level LNP delivery. Spleens were stained for the cell surface markers CD45, CD3, CD19, CD11b, and CD11c in order to quantify LNP accumulation on a single cell level using flow cytometry.

Approximately 52% of $CD45^+/CD11b^+$ myeloid cells were DiR^+ with no significant differences observed between LNP treatment groups (Fig. 6C). Roughly 42% and 38% of $CD45^+/CD11b^+/CD11c^+$ dendritic cells were DiR^+ following treatment with LNP A1 and 1:5 aEGFR-LNPs respectively (Fig. 6D). These results are consistent with previous work, which have reported LNP accumulation in $CD11b^+$ myeloid and $CD11b^+/CD11c^+$ dendritic cells, likely due to LNP opsonization and phagocytosis by the MPS [10,71,72]. Given the enhanced bioluminescence observed in spleens during biodistribution experiments with 1:5 aEGFR-LNPs, we suspected that functionalization of LNPs with antibodies could potentially lead to increased recognition and internalization by splenic macrophages and immune cells of the MPS. However, DiR positivity in $CD45^+/CD11b^+$ and $CD45^+/CD11b^+/CD11c^+$ cells was not significantly different between LNP A1 and 1:5 aEGFR-LNPs, suggesting that the presence of EGFR antibodies on LNPs at an intermediate density does not exacerbate phagocytic action by splenic immune cells.

Around 8% of splenic $CD45^+/CD3^+$ T cells were DiR^+ across both LNP treatment groups (**Fig. S12**). Interestingly, treatment with 1:5 aEGFR-LNPs resulted in a significant reduction in uptake in $CD45^+/CD19^+$ B cells, with approximately 6% and 3% DiR^+ B cells observed with LNP A1 and 1:5 aEGFR-LNPs respectively (Fig. 6E). As splenic immune cells play a vital role in innate and adaptive immune responses against foreign alloantigens [62], the observed similarities in accumulation of 1:5 aEGFR-LNPs and LNP A1 in $CD11b^+$ and $CD11b^+/CD11c^+$ antigen-presenting cells may suggest that the presence of EGFR antibodies on LNPs does not elicit an exacerbated immune response when compared to the non-targeted LNP A1. Rather, the comparable accumulation of 1:5 aEGFR-LNPs and LNP A1 in splenic immune cells may speak to a potentially enhanced safety profile of aEGFR-LNPs during pregnancy due to a diminished maternal immune responsiveness to foreign antibodies and a resultant decrease in antibody trafficking to immune cells in the spleen. Additional work is required to further elucidate mechanisms of antibody-mediated immunoreactivity during pregnancy.

Finally, to further investigate the safety profile of engineered aEGFR-LNPs, we selected a panel of inflammatory cytokines and measured the relative concentration of each cytokine in serum from PBS-treated mice compared to LNP-treated mice (Fig. 6I). As a benchmark to other LNP platforms, we also measured serum levels of the secreted liver enzymes alanine aminotransferase (ALT) and aspartate aminotransferase (AST) to probe for any potential LNP-mediated liver toxicity (**Fig. S13**). 12 h after LNP administration, there were no significant changes in ALT or AST levels in LNP-treated mice compared to PBS-treated mice. Similarly, at 12 h, relative levels of the common inflammation markers interleukin 1-alpha (IL-1α), interleukin 1-beta (IL-1β), granulocyte-macrophage colony-stimulating factor (GM-CSF), macrophage inflammatory protein 1-alpha (MIP-1α), and stem cell factor (SCF) did not differ between PBS-treated and LNP-treated mice. Levels of monocyte chemoattractant protein-1 (MCP-1) and RANTES were significantly higher in LNP-treated mice compared to PBS-treated mice; however, cytokine levels did not significantly differ between LNP treatment groups. Granulocyte colony-stimulating factor (G-CSF) levels were also significantly higher in LNP-treated mice compared to PBS-treated mice, however relative G-CSF levels were significantly higher with 1:5 aEGFR-LNPs compared to LNP A1. Increased levels of MCP-1, RANTES, and G-CSF have all previously been reported following administration of mRNA LNPs, as elevation of these cytokines has been implicated in the innate immune response to foreign nucleic acids [71]. Thus, the relative increase in MCP-1, RANTES, and G-CSF levels in LNP-treated mice compared to PBS-treated mice are potentially a reaction to the presence of foreign mRNA. The additional increase in G-CSF levels observed with 1:5 aEGFR-LNPs compared to LNP A1 suggests an increase in neutrophil activity in the presence of antibody-conjugated LNPs, as the primary role of G-CSF is regulation of neutrophil proliferation and trafficking. More specifically, it has been reported that neutrophil expression of high-affinity Fc receptors increases in the presence of G-CSF [73] and, thus, increased levels of G-CSF may be indicative of neutrophil recruitment for downstream opsonization of antibody-conjugated LNPs. Neutrophil activation has been previously reported following LNP administration, and is, importantly, a transient response, with G-CSF levels and neutrophil activation typically returning to baseline levels on the order of 48–72 h [15,71]. Given that the dosages used in this work are consistent with those being investigated in clinical trials [74], we believe these data support that aEGFR-LNPs do not substantially exacerbate the inflammatory immune response in mice when compared to other LNP formulations and highlight the safety of 1:5 aEGFR-LNPs for targeted mRNA delivery to the placenta during pregnancy.

2.6. aEGFR-LNPs enhance uptake in placental trophoblasts and immune cells

Given that one of the main advantages conferred by targeted LNPs is their ability to promote LNP uptake in specific receptor-expressing cells, we sought to evaluate uptake and accumulation of our lead placenta-tropic LNP formulation, 1:5 aEGFR-LNPs, on a cellular level in murine placentas compared to LNP A1. To probe cellular-level uptake in the placenta, DiR-labeled LNPs were administered to pregnant mice at a dose of 1 mg of mRNA per kg body mass *via* tail vein injection. Mice were euthanized 12 h after injection and placentas and fetuses were imaged using IVIS.

DiR fluorescence flux in the placentas was significantly higher with 1:5 aEGFR-LNPs compared to LNP A1, suggesting that engineered aEGFR-LNPs promote increased accumulation in placentas during pregnancy (Fig. 6B, **Fig. S14).** DiR fluorescence was not detected in fetuses (**Fig. S14**). After imaging, placentas were processed to generate single cell suspensions and examined for DiR fluorescence *via* flow cytometry. Because results from our biodistribution experiments validated the ability of 1:5 aEGFR-LNPs to induce luciferase expression in placentas, we again chose to evaluate DiR fluorescence as a metric of LNP uptake in the placenta to determine whether aEGFR-LNPs

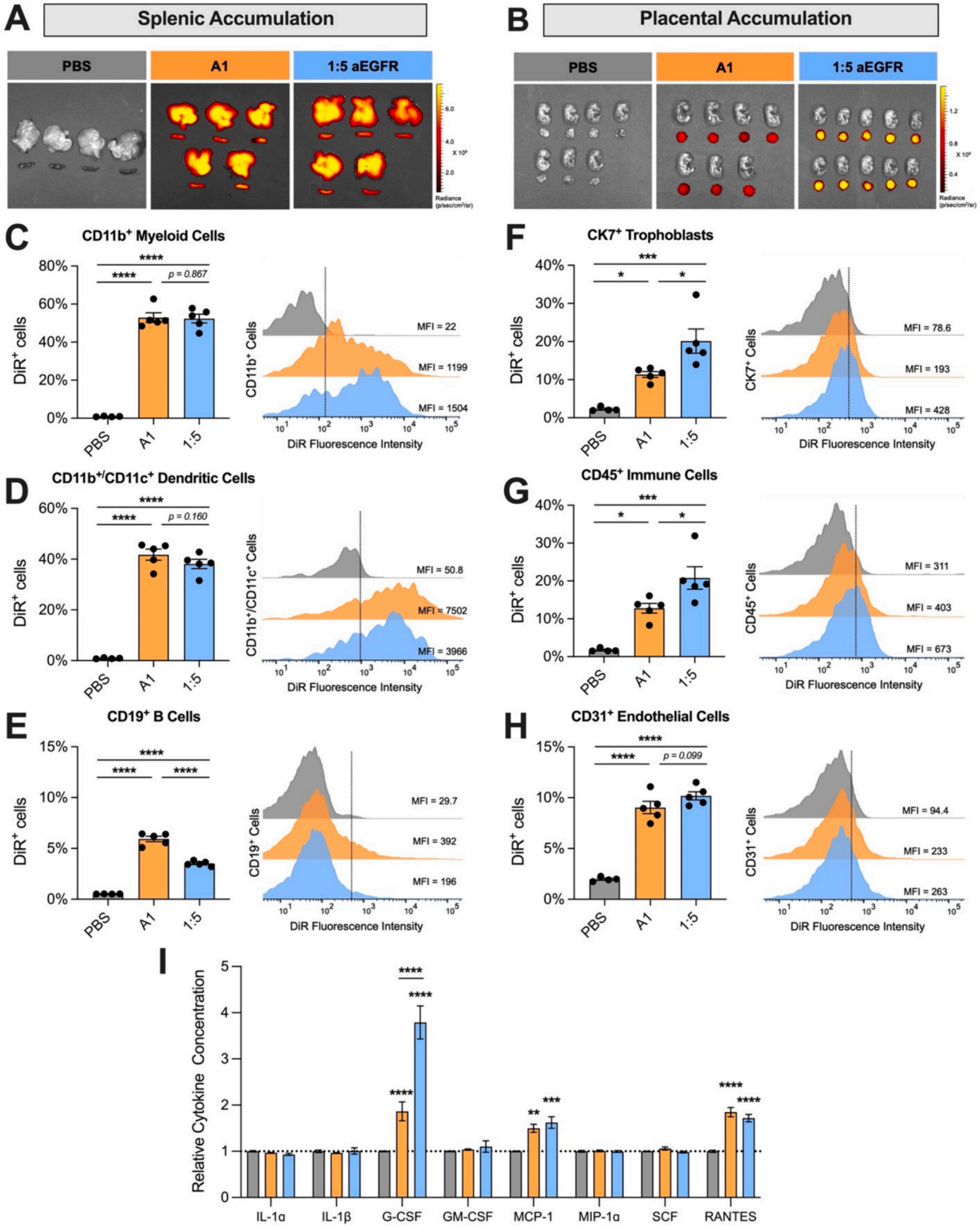

(caption on next page)

Fig. 6. ***In vivo*** **splenic and placental accumulation of DiR-labeled aEGFR-LNPs. (A,B)** Fluorescence IVIS images of DiR-labeled LNP A1 or 1:5 aEGFR-LNP accumulation (1 mg mRNA/kg body mass) in the **(A)** livers and spleens and **(B)** placentas and fetuses of pregnant mice. Spleens and placentas were further analyzed *via* flow cytometry. Quantification and representative histograms of DiR^+ cells in **(C)** $CD45^+/CD11b^+$ myeloid cells, **(D)** $CD45^+/CD11b^+/CD11c^+$ dendritic cells, **(E)** $CD45^+/CD19^+$ B cells in the spleen, **(F)** $CK7^+$ trophoblasts, **(G)** $CD45^+$ immune cells, and **(H)** $CD31^+$ endothelial cells in the placentas. Percent DiR^+ cells in the spleen and placentas are reported as mean ± SEM from $n = 4$ and $n = 5$ biological replicates for PBS-treated and LNP-treated mice respectively with $n = 3$–8 placentas and fetuses per mouse. Representative histograms are shown from samples with the DiR^+ cell proportion closest to the mean for each treatment group. One-way and nested one-way ANOVA with *post hoc* Student's *t*-test using the Holm–Šídák correction for multiple comparisons were used to compare percent DiR+ cells across treatment groups in the spleen and placentas respectively. **(I)** Cytokine levels in serum 12 h following treatment with PBS, LNP A1, or 1:5 aEGFR-LNPs. For each cytokine, data are normalized to the average of the optical density measurements for PBS-treated mice (dashed line). Cytokine data are reported as mean ± SEM from $n = 4$ biological replicates. Two-way ANOVA with *post hoc* Student's *t*-tests using the Holm–Šídák correction for multiple comparisons was used to compare relative concentration across cytokines and LNP treatment groups. $^*p \leq 0.05$, $^{**}p \leq 0.01$, $^{***}p \leq 0.001$, $^{****}p \leq 0.0001$.

demonstrate altered cellular accumulation compared to LNP A1. Placentas were stained for the cell surface markers CD45 and CD31 and the intracellular marker CK7 to assess LNP accumulation on a single cell level using flow cytometry.

1:5 aEGFR-LNPs doubled the observed proportion of DiR^+ $CK7^+$ trophoblasts compared to LNP A1, confirming that LNPs targeted to EGFR-expressing trophoblasts can not only traffic to the placenta but also increase LNP internalization in designated EGFR-expressing cell types. Approximately 10% and 20% of trophoblasts were DiR^+ following treatment with LNP A1 and 1:5 aEGFR-LNPs respectively (Fig. 6F), demonstrating a significant increase in LNP accumulation in $EGFR^+$ trophoblasts *via* active EGFR targeting.

1:5 aEGFR-LNPs also demonstrated a significant increase in uptake in $CD45^+$ immune cells (20% DiR^+) when compared to LNP A1 (13% DiR^+), likely due to the high presence of immune cells at the maternal-fetal interface [75] (Fig. 6G). Given that placental immune cells are a key mediator in many placental disorders, including preeclampsia [19], enhanced uptake of aEGFR-LNPs in placental immune cells could confer additional benefits for treating these conditions. Around 10% of $CD31^+$ endothelial cells in the placenta were DiR^+ regardless of treatment group (Fig. 6H). Taken together, these results demonstrate that EGFR antibody conjugation at an intermediate density improves mRNA delivery to the placenta during healthy pregnancy, and more specifically, that IV administered 1:5 aEGFR-LNPs enhance LNP uptake twofold in $EGFR^+$ trophoblasts in the placenta during pregnancy.

3. Conclusions

In this work, we utilized SPAAC to engineer EGFR antibody-conjugated LNPs to enhance mRNA delivery to the placenta during pregnancy. Our top performing LNP (1:5 aEGFR-LNP) with an intermediate density of antibody functionalization demonstrated enhanced *in vivo* luciferase mRNA delivery in murine placentas compared to non-targeted LNP A1, with a comparable safety profile to the non-targeted LNP A1 and no fetal luminescence observed. Further, cellular-level examination revealed a ~twofold increase in uptake of 1:5 aEGFR-LNPs in EGFR-expressing trophoblasts in the placenta compared to the non-targeted LNP A1. Together, these results demonstrate the potential of antibody-conjugated LNPs to promote LNP trafficking to EGFR-expressing cells in the placenta.

Previous reports have established the importance of antibody clone in the design of antibody-conjugated nanoparticle drug delivery platforms [36,76]. Specifically, the selected antibody clone can exert drastic effects on the efficacy of an actively targeted system, potentially due to differences in antigen binding affinity and whether the antibody clone exhibits antagonistic or non-antagonistic binding behavior [36]. In this work, we selected a widely accessible off-the-shelf anti-EGFR antibody for simplicity and reproducibility. However, the targeting efficacy of our aEGFR-LNPs could potentially be improved by optimizing the antibody clone. Future work could evaluate various antibody clones against EGFR to identify those that are capable of promoting potent LNP uptake in EGFR-expressing cells in the placenta.

Similarly, changes in receptor expression during disease progression may also affect the efficacy of targeted LNP systems. Given that many placental dysfunction disorders, including preeclampsia, are marked by overexpression of pathologic cellular receptors, antibody-conjugated LNPs have the potential to exert even more robust targeting during pregnancies complicated by placental dysfunction. For example, in this work, 1:5 aEGFR-LNPs resulted in a ~twofold increase in LNP uptake in EGFR-expressing trophoblasts during healthy pregnancy. However, recent work has suggested that systemic endothelial dysfunction present during preeclampsia may arise from an upregulation of EGFR in placental endothelial cells, which do not express EGFR under healthy conditions [48]. During preeclamptic pregnancies, aEGFR-LNPs could potentially promote uptake of mRNA LNPs in both trophoblasts and placental endothelial cells, thereby enhancing their overall therapeutic efficacy. Here, we have demonstrated the ability of 1:5 aEGFR-LNPs to facilitate potent mRNA delivery and enhanced LNP uptake in EGFR-expressing cells in the placenta during healthy pregnancy. Future work should investigate aEGFR-LNP-mediated delivery of therapeutically relevant pro-angiogenic mRNA cargos, such as vascular endothelial growth factor (VEGF) or placental growth factor (PlGF) [15,17], in a model of placental dysfunction for applications in treating obstetric complications.

Finally, in this work, we have demonstrated the safety profile of 1:5 aEGFR-LNPs during pregnancy. However, it is well appreciated that engineered antibody fragments, such as single chain variable fragments (ScFv), offer additional benefits over whole antibodies, including smaller size and lack of immunogenic Fc regions [77]. While Fc regions may potentially be less immunogenic during pregnancy due to reduced allogenic immune responses, the removal of Fc regions could further enhance the safety profile of aEGFR-LNPs, which may be particularly important during obstetric complications marked by inflammation at the maternal-fetal interface. Deeper investigations into the mechanisms driving antibody trafficking and Fc immunogenicity *in vivo* in both non-pregnant and pregnant models will enable the full realization of antibody-conjugated LNP platforms in achieving targeted, extrahepatic nucleic acid delivery for a range of therapeutic applications including for pregnancy disorders.

4. Materials and methods

4.1. Ionizable lipid synthesis

The C12–494 ionizable lipid was synthesized as previously described [15]. Briefly, the polyamine core 2-{2-[4-(2-{[2-(2 aminoethoxy)ethyl] amino}ethyl)piperazin-1-yl]ethoxy}ethan-1-amine (Enamine, Kyiv, Ukraine) was reacted with an excess epoxide tail 1,2-epoxydodecane (MilliporeSigma, Burlington, MA) for 48 h at 80 °C. Ethanol was evaporated using a Rotovapor R-300 rotary evaporator (Buchi, New Castle, DE) and the crude product was resuspended in ethanol for lipid nanoparticle (LNP) formulation.

4.2. mRNA production

Luciferase mRNA with 5-methoxyuridine modifications and mCherry mRNA with N^1-methylpseudouridine modifications were purchased from Trilink Biotechnologies (San Diego, CA) for *in vitro* screening

experiments and *in vivo* cell-specific flow cytometry experiments, respectively. For *in vivo* biodistribution experiments, luciferase mRNA was synthesized with the pseudouridine modification using *in vitro* transcription as previously described [78].

4.3. Protein modification and purification

Anti-human (mouse anti-human, AY13, Biolegend, San Diego, CA) or anti-mouse (rabbit anti-mouse, 30H45L48, ThermoFisher Scientific, Waltham, MA) EGFR antibodies were concentrated using 10 kDa molecular weight filter columns (Abcam, Cambridge, UK) in azide-free phosphate buffered saline (PBS). Antibodies were then functionalized with dibenzocyclooctyne (DBCO) *via* incubation with a 30-fold molar excess of TFP-PEG(4)-DBCO (ThermoFisher Scientific) in anhydrous DMSO for 2 h at room temperature. Unreacted TFP-PEG(4)-DBCO was removed using Zeba Dye and Biotin Removal spin columns (ThermoFisher Scientific). Final protein concentration was measured using a Qubit Protein Quantification Assay (ThermoFisher Scientific). The purified DBCO-labeled antibodies were stored at 4 °C for later use.

4.4. Lipid nanoparticle formulation

LNPs were synthesized *via* microfluidic mixing at a weight ratio of 10:1 of ionizable lipid to mRNA as previously described [6]. The ionizable lipid C12–494 was combined in an ethanol phase with 1,2-dioleoyl-sn-glycero-3-phosphoethanolamine (DOPE, Avanti Polar Lipids, Alabaster, AL), cholesterol (Sigma Aldrich, St. Louis, MO), 1,2-dimyristoyl-*sn*-glycero-3-phosphoethanolamine-N-[methoxy(polyethylene glycol)-2000] (ammonium salt) (C14-PEG_{2000}, Avanti Polar Lipids), and 1,2-distearoyl-sn-glycero-3-phosphoethanolamine-N-[azido(polyethylene glycol)-2000] (ammonium salt) (DSPE- PEG_{2000}-azide, Avanti Polar Lipids) at a molar ratio of 35 ionizable lipid: 16 DOPE: 46.5 Cholesterol: 2.5 total PEG, where the ratio of DSPE-PEG-azide: C14-PEG_{2000} varied as described in **Table S1**. To form the aqueous phase, 25 μg of luciferase mRNA or mCherry mRNA was dissolved in 10 mM citrate buffer (pH = 3) to form an aqueous phase. The ethanol and aqueous phases were combined in a microfluidic device at a 1:3 volumetric ratio using syringe pumps (Harvard Apparatus, Holliston, MA) to induce chaotic mixing. After formulation, LNPs were dialyzed against 1X PBS for 2 h in cassettes with a 20 kDa molecular weight cutoff filter (Thermo Fisher Scientific). LNPs were then sterilized with 0.22 μm filters and conjugated with antibodies. Non-targeted controls LNP S1 and LNP A1 were sterilized and then stored at 4 °C for later use.

4.5. Generation of antibody-conjugated LNPs

To functionalize LNPs with antibody, DBCO-labeled antibody was incubated with azide-containing LNPs at a 5-fold molar excess for 4 h at 25 °C with gentle shaking and then left to incubate overnight at 4 °C to complete the reaction. Antibody-conjugated LNPs were purified using size exclusion chromatography. Briefly, a column was packed with Sepharose CL-6B (Sigma Aldrich) and rinsed with 1X PBS to clear ethanol from the system. Antibody-conjugated LNPs were passed through the column and collected in ~200 μL fractions. Collected fractions were measured *via* A260/A280 reading on an Infinite 200 Pro plate reader (Tecan, Morisville, NC); all fractions containing mRNA were pooled and concentrated using 100 kDa filters (Sigma Aldrich). The final LNP solution was stored at 4 °C for later use.

4.6. Lipid nanoparticle characterization

Following antibody conjugation, the mRNA concentration of each LNP formulation was measured using a Quant-iT-RiboGreen RNA assay (ThermoFisher Scientific). In a nuclease-free environment, each LNP formulation was diluted 80X in either 1X tris-EDTA (TE) buffer or TE buffer containing 0.1% (*v*/v) Triton X-100 (Sigma Aldrich). LNPs were shaken at 350 rpm for 20 min at room temperature to facilitate particle lysis. LNPs in TE buffer, LNPs in Triton-X-100, and RNA standards were plated in triplicate in black bottom 96 well plates and Ribogreen fluorescent detection reagent was added to each well per manufacturer instructions. After incubation for 5 min at room temperature, the fluorescence intensity was read on an Infinite 200 Pro plate reader (Tecan) at an excitation/emission of 480/520 nm. Encapsulation efficiencies were measured as percent change between lysed LNPs in Triton X-100 and non-lysed LNPs in TE buffer. mRNA concentrations of LNP formulations were estimated by comparison to a standard curve fit calculated using least squares linear regression. Encapsulation efficiencies and mRNA concentration are reported as mean ± standard deviation of $n = 3$ replicates.

LNP size was determined *via* dynamic light scattering measurements (DLS). LNPs were diluted 12X in 1X PBS in a 384 well plate and read on a DynaPro Plate Reader III (Wyatt Technology, Santa Barbara, CA). Zeta potential measurements were conducted using a Zetasizer Nano (Malvern Instruments, Malvern, UK). LNPs were diluted 50X in ultrapure water in disposable folded capillary cells (Malvern Instruments). For each sample, three measurements with five runs were recorded. *Z*-average size, polydispersity index (PDI) and zeta potential are reported as mean ± standard deviation of $n = 3$ replicates.

LNP antibody concentration was determined using a Microscale Protein Labeling Kit (ThermoFisher Scientific). EGFR antibodies were dual functionalized with DBCO and Alexa Fluor 647 at a 1:1 molar equivalent for 1 h at room temperature. Dual functionalized antibodies were then incubated with azide-containing LNPs at a 5-fold molar excess for 4 h at 25 °C with gentle shaking and then left to incubate overnight at 4 °C to complete the reaction. After size exclusion chromatography, antibody-conjugated LNPs were plated in black bottom 96 well plates alongside standard curves generated with dual functionalized antibodies alone. Fluorescence intensity was read on an Infinite 200 Pro plate reader (Tecan) at an excitation/emission of 638/668 nm. LNPs conjugated to non-fluorescently tagged antibodies were included as a negative control, with no background fluorescence detected.

The pK_a values of each LNP formulation were determined from a 6-(p-toluidinyl) naphthalene-2-sulfonic acid (TNS) assay. TNS reagent was diluted in ultrapure water to a concentration of 0.16 mM. Buffered solutions of 150 mM sodium chloride, 20 mM sodium phosphate, 25 mM ammonium citrate and 20 mM ammonium acetate were adjusted to a pH between 2 and 12 at 0.5 increments. LNPs were added to each pH adjusted solution and plated in triplicate in a black bottom 96-well plate. Diluted TNS solution was added to each well for a final TNS concentration of 6 μM. The fluorescence intensity was measured using an Infinite 200 Pro plate reader (Tecan) at an excitation/emission of 322/431 nm. The pK_a value of each LNP formulation was calculated at 50% protonation, represented by the pH at which the fluorescence intensity reached 50% of its maximum value.

4.7. In vitro LNP-mediated luciferase mRNA delivery to JEG-3 placental cells

JEG-3 choriocarcinoma cells (ATCC #HTB-36, Manassas, VA) were cultured in Dulbecco's Modified Eagle Medium supplemented with 10% FBS (DMEM, Gibco, Dublin, Ireland) and 1% penicillin-streptomycin (Gibco) and maintained at 37 °C and 5% CO_2. For all experiments, JEG-3 cells were plated at a density of 50,000 cells/well in 100 μL Opti-MEM Reduced Serum Medium (Gibco) in tissue-culture treated 96-well plates and then left to adhere overnight. To assess LNP-mediated luciferase expression *in vitro,* cells were treated with 50 ng of mRNA per 50,000 cells. After 24 h, media was removed, and cells were incubated with 0.1% Triton-X for 3 min. 100 μL of luciferase assay substrate (Promega, Madison, WI) was then added to each well, and cells were left to incubate at room temperature for 10 min. Luminescence was detected using an Infinite 200 Pro plate reader (Tecan). Normalized luciferase expression for each treatment group was calculated by first subtracting

the background readings from untreated cells and then by dividing by the average luminescence signal from the control azide formulation (LNP A1) treated wells. Normalized luciferase expression is reported as mean ± standard deviation of the mean (SEM) from $n = 5$ biological replicates (averaged from $n = 5$ technical replicates each).

To evaluate LNP-mediated cytotoxicity, JEG-3 cells were plated and dosed as described above. After 24 h, 100 μL of CellTiter-Glo (Promega) was added to each well. Cells were incubated for 10 min at room temperature, and luminescence was quantified using a plate reader. The luminescence signal for each treatment group was normalized to untreated wells. Percent cell viability is reported as mean ± standard deviation of the mean (SEM) from $n = 5$ biological replicates (averaged from $n = 5$ technical replicates each).

For dose response experiments, JEG-3 cells were plated and dosed at 10, 25, 50, 100, and 250 ng of mRNA per 50,000 cells. Luciferase expression and cytotoxicity were measured as described above. Normalized luciferase expression and percent cell viability are reported as mean ± SEM from $n = 5$ biological replicates (averaged from $n = 3$ technical replicates each).

4.8. Animal experiments

All animal use was in accordance with the guidelines and approval from the University of Pennsylvania's Institutional Animal Care and Use Committee (IACUC, protocol #806540). Non-pregnant female mice (8–12 weeks old, approximately 20 g average weight) and time-dated pregnant female mice (varied age, approximately 30 g average weight) were purchased from the Jackson Laboratory (Bar Harbor, ME).

4.9. LNP-mediated in vivo luciferase mRNA delivery to non-pregnant and pregnant mice

LNPs encapsulating luciferase mRNA were administered to non-pregnant and gestational day E16 pregnant mice *via* an intravenous injection of the tail vein at a dose of 0.4 mg of mRNA per kg body mass. PBS injections were used as a control. 6 h following administration, mice received an intraperitoneal injection of *D*-luciferin potassium salt (Regis Technologies, Morton Grove, IL) at a dose of 150 mg of *D*-luciferin per kg body mass (Biotium, Fremont, CA). After 10 min, mice were euthanized with CO_2 and the heart, lung, liver, kidneys, spleen, and uterus were removed. In pregnant mice, the uteruses were dissected to remove the fetuses and placentas. Luminescence imaging of the organs was performed using an *in vivo* imaging system (IVIS, PerkinElmer, Waltham, MA).

To quantify luminescence flux, the Living Image software (PerkinElmer) was used to place a rectangular region of interest (ROI) around the organ or fetus of interest. An equal sized ROI was placed in an area without any luminescence signal on the same image. Normalized flux was calculated by subtracting the total flux of the background ROI from the total flux of the organ or fetus. Reported bioluminescence for the maternal organs are reported as mean ± SEM from $n = 5$ biological replicates. Bioluminescence for the placentas and fetuses are reported as mean ± SEM from $n = 5$ biological replicates with $n = 3$–9 placentas and fetuses per mouse depending on litter size.

4.10. Cell-specific accumulation of DiR-labeled LNPs in spleens and placentas in pregnant mice

LNPs encapsulating mCherry mRNA were labeled with 1% (*v*/v) DiR Cell-Labeling Solution (ThermoFisher Scientific) for 15 min at 25 °C with gentle shaking at 300 rpm. Gestational day E16 pregnant mice were intravenously injected *via* the tail vein with DiR-labeled mCherry LNPs or PBS at a dose of 1 mg of mRNA per kg body mass. After 12 h, mice were euthanized with CO_2 and the liver, spleen, and uterus were removed. The uteruses were dissected to remove the fetuses and placentas. Fluorescence intensity imaging was performed using IVIS with a filter paired for DiR, and fluorescence flux was calculated using ROIs as described above. Reported fluorescence for the spleen represents the mean ± SEM from $n = 4$–5 biological replicates. Reported fluorescence for the placentas and fetuses represents the mean ± SEM from $n = 4$–5 biological replicates each with $n = 6$–10 placentas and fetuses per mouse depending on litter size. Statistical analyses for fluorescence flux are the same as those described above.

Following imaging, placentas and spleens were collected into 2 mL deionized water and 2 mL 1% PBSA +2 mM EDTA, respectively, and placed on ice. Organs were digested through 100 μm cell strainers (ThermoFisher Scientific) to form single cell suspensions. Placenta suspensions were incubated with 200 μL of 10X DNase I buffer (New England BioLabs, Ipswich, MA) and 20 μL of 2000 U/mL DNase I (New England BioLabs) for 30 min at room temperature. Placenta and spleen samples were then incubated with ACK lysis buffer (ThermoFisher Scientific) for 5 min. Samples were spun at 300 *g* for 5 min, and supernatant was aspirated. This step was repeated until red blood cells were completely removed from the sample. Cell pellets were resuspended in 1% PBSA +2 mM EDTA. Samples were blocked with 0.5 μL of TruStain FcX PLUS (anti-mouse CD16/32) antibody (BioLegend) for 10 min on ice.

Placenta samples were first stained for extracellular surface markers for 30 min at 4 °C with 3 μL of APC anti-mouse CD45 antibody and 3 μL of Brilliant Violet 421 anti-mouse CD31 antibody (BioLegend). Placenta samples were then washed, fixed, and permeabilized using the Cyto-Fast Fix/Perm buffer kit (BioLegend) per the manufacturer's instructions before undergoing intracellular staining with 1 μL of FITC anti-mouse cytokeratin-7 antibody (Novus Biologicals, Littleton, CO).

Spleen samples were stained for cell surface markers for 30 min at 4 °C with 1.5 μL of Spark 387 anti-mouse CD45 antibody, 3 μL of APC anti-mouse CD3 antibody, 1.5 μL of Pacific Blue anti-mouse CD19 antibody, 3 μL of Alexa Fluor 488 anti-mouse CD11b antibody, and 6 μL of Brilliant Violet 711 anti-mouse CD11c antibody (BioLegend).

Data was acquired using a BD LSR Fortessa Cytometer equipped with UV, violet, blue, yellow-green, and red lasers. For each sample, at least 30,000 events within the singlet gate were collected. Thresholds for positivity were determined using fluorescence-minus-one (FMO) controls with representative gating schemes for the spleen and placenta found in the Supplementary Information (**Fig. S15,16**). The percent of DiR^+ $CD3^+$ T cells, $CD19^+$ B cells, $CD11b^+$ myeloid cells, and $CD11c^+$ dendritic cells in the spleen are reported as the mean ± SEM from $n = 4$–5 biological replicates. One-way ANOVA with *post hoc* Student's *t*-tests using the Holm-Šídák correction for multiple comparisons was used to compare the percent of DiR^+ cells across treatment groups in the spleen. The percent of DiR^+ $CK7^+$ trophoblasts, $CD45^+$ immune cells, and $CD31^+$ endothelial cells in the placenta are reported as the mean ± SEM from $n = 4$–5 biological replicates with $n = 3$–8 placentas each depending on litter size. Nested one-way ANOVA with *post hoc* Student's *t*-tests using the Holm-Šídák correction for multiple comparisons was used to compare the percent of DiR^+ cells across treatment groups in the placentas. Representative histograms are shown for both the placenta and spleen with values for the percent of DiR^+ cells closest to the mean for each treatment group.

4.11. In vivo LNP-mediated inflammation and toxicity in pregnant mice

Gestational day E16 pregnant mice were intravenously injected *via* the tail vein with DiR-labeled mCherry LNPs or PBS at a dose of 1 mg of mRNA per kg body mass. After 12 h, blood was collected *via* retro orbital bleeding into Microtainer blood collection tubes (BD, Franklin Lakes, NJ). Blood was allowed to clot for 2 h at room temperature and then centrifuged for 20 min at 2000 *g*. Serum was removed, aliquoted, and stored at −20 °C for later use. A colorimetric Mouse Inflammation ELISA kit (Signosis, Santa Clara, CA) was used to evaluate IL-1α, IL-1β, G-CSF, GM-CSF, MCP-1, MIP-1α, SCF, and RANTES levels in serum 12 h after LNP administration per the manufacturer's instructions. For each

cytokine, the reported measurements for relative cytokine concentration are normalized to the average optical density measurements from the PBS-treated group. Data represent the mean ± SEM from $n = 4$ biological replicates with $n = 1$ technical replicate per cytokine. Colorimetric assay kits (Cayman Chemical, Ann Arbor, MI) were used to evaluate serum levels of alanine aminotransferase (ALT) and aspartate aminotransferase (AST) 12 h after LNP administration per the manufacturer's instructions. Data represent the mean ± SD from $n = 3$ biological replicates with $n = 3$ technical replicates each. Two-way ANOVA with *post hoc* Student's *t*-tests using the Holm-Šídák correction for multiple comparisons was used to compare relative serum levels or enzyme levels across treatment groups.

4.12. Statistical analysis

All statistical analyses were performed using GraphPad Prism. For experiments screening LNPs for *in vitro* luciferase expression and cell viability, nested one-way ANOVA with *post hoc* Student's *t*-tests using the Holm–Šídák correction for multiple comparisons was used to compare the luciferase expression or cell viability across treatment groups to LNP A1. For *in vivo* luminescence flux measurements in the maternal organs following LNP delivery to non-pregnant and pregnant mice, ordinary one-way ANOVA with *post hoc* Student's *t*-tests using the Holm–Šídák correction for multiple comparisons was used to compare the luciferase expression in livers and spleens and other maternal organs across treatment groups to LNP A1, and two-way ANOVA with *post hoc* Student's *t*-tests using the Holm–Šídák correction for multiple comparisons was used to compare luminescence flux in uteruses across LNP treatment groups in non-pregnant *vs.* pregnant mice. For *in vivo* luminescence flux measurements in placentas and fetuses following LNP delivery to pregnant mice, nested one-way ANOVA with *post hoc* Student's *t*-tests using the Holm–Šídák correction for multiple comparisons was used to compare flux across treatment groups. For *in vivo* DiR-labeled LNP cellular-level accumulation experiments in the spleen and placentas, ordinary and nested one-way ANOVA were used respectively with *post hoc* Student's t-tests using the Holm- Šídák correction for multiple comparisons to compare DiR positivity across treatment groups. For cytokine analysis, two-way ANOVA with *post hoc* Student's *t*-tests using the Holm–Šídák correction for multiple comparisons was used to compare relative concentration across cytokines and LNP treatment groups. For all figures, statistical significance is denoted by $*p \leq 0.05$, $**p \leq 0.01$, $***p \leq 0.001$ and $****p \leq 0.0001$.

CRediT authorship contribution statement

Hannah C. Geisler: Writing – review & editing, Writing – original draft, Visualization, Methodology, Formal analysis, Data curation, Conceptualization. **Aditi A. Ghalsasi:** Data curation. **Hannah C. Safford:** Data curation. **Kelsey L. Swingle:** Data curation. **Ajay S. Thatte:** Data curation. **Alvin J. Mukalel:** Data curation. **Ningqiang Gong:** Data curation. **Alex G. Hamilton:** Data curation. **Emily L. Han:** Data curation. **Benjamin E. Nachod:** Data curation. **Marshall S. Padilla:** Data curation. **Michael J. Mitchell:** Supervision, Resources, Funding acquisition, Conceptualization.

Declaration of competing interest

H.C.G., K.L.S., H.C.S., and M.J.M. have filed a patent application related to this study. The remaining authors declare no competing interests.

Data availability

Data will be made available on request.

Acknowledgements

The authors acknowledge and thank the Penn Cytomics and Cell Sorting Core (RRID: SCR_022376). M.J.M. acknowledges support from a National Institutes of Health (NIH) Director's New Innovator Award (no. DP2TR002776), a National Science Foundation (NSF) CAREER Award (no. CBET-2145491), and a Burroughs Wellcome Fund Career Award at the Scientific Interface. H.C.G, H.C.S., K.L.S., A.S.T., A.J.M., A.G.H., and E.L.H. were supported by National Science Foundation Graduate Research Fellowships (Award 1845298). M.S.P. was supported by the National Institute of Dental & Craniofacial Research (NIDCR) of the NIH (no. T90DE030854) and the Center for Innovation & Precision Dentistry (CiPD) at the University of Pennsylvania.

Author contributions

H.C.G. and M.J.M. conceived and designed the experiments. The experiments were performed by H.C.G., A.A.G., H.C.S., K.L.S., A.S.T., A. J.M., N.G., A.G.H., E.L.H., B.E.N., M.S.P. and interpreted by all authors. H.C.G and M.J.M. wrote the manuscript. All authors edited the manuscript and approved the final version for submission.

Appendix A. Supplementary data

Supplementary data to this article can be found online at https://doi.org/10.1016/j.jconrel.2024.05.036.

References

[1] X. Hou, T. Zaks, R. Langer, Y. Dong, Lipid nanoparticles for mRNA delivery, Nat. Rev. Mater. 6 (2021) 1078–1094, https://doi.org/10.1038/s41578-021-00358-0.
[2] K.L. Swingle, A.G. Hamilton, M.J. Mitchell, Lipid nanoparticle-mediated delivery of mRNA therapeutics and vaccines, Trends Mol. Med. 27 (2021) 616–617, https://doi.org/10.1016/j.molmed.2021.03.003.
[3] K. Garber, Alnylam launches era of RNAi drugs, Nat. Biotechnol. 36 (2018) 777–778, https://doi.org/10.1038/nbt0918-777.
[4] H. Yin, R.L. Kanasty, A.A. Eltoukhy, A.J. Vegas, J.R. Dorkin, D.G. Anderson, Non-viral vectors for gene-based therapy, Nat. Rev. Genet. 15 (2014) 541–555, https://doi.org/10.1038/nrg3763.
[5] A.G. Hamilton, K.L. Swingle, M.J. Mitchell, Biotechnology: overcoming biological barriers to nucleic acid delivery using lipid nanoparticles, PLoS Biol. 21 (2023) e3002105, https://doi.org/10.1371/journal.pbio.3002105.
[6] K.J. Kauffman, J.R. Dorkin, J.H. Yang, M.W. Heartlein, F. DeRosa, F.F. Mir, O. S. Fenton, D.G. Anderson, Optimization of lipid nanoparticle formulations for mRNA delivery in vivo with fractional factorial and definitive screening designs, Nano Lett. 15 (2015) 7300–7306, https://doi.org/10.1021/acs.nanolett.5b02497.
[7] K.A. Hajj, K.A. Whitehead, Tools for translation: non-viral materials for therapeutic mRNA delivery, Nat. Rev. Mater. 2 (2017) 1–17, https://doi.org/10.1038/natrevmats.2017.56.
[8] R. Zhang, R. El-Mayta, T.J. Murdoch, C.C. Warzecha, M.M. Billingsley, S. J. Shepherd, N. Gong, L. Wang, J.M. Wilson, D. Lee, M.J. Mitchell, Helper lipid structure influences protein adsorption and delivery of lipid nanoparticles to spleen and liver, biomaterials, Science 9 (2021) 1449–1463, https://doi.org/10.1039/D0BM01609H.
[9] S. Muro, C. Garnacho, J.A. Champion, J. Leferovich, C. Gajewski, E.H. Schuchman, S. Mitragotri, V.R. Muzykantov, Control of endothelial targeting and intracellular delivery of therapeutic enzymes by modulating the size and shape of ICAM-1-targeted carriers, Mol. Ther. 16 (2008) 1450–1458, https://doi.org/10.1038/mt.2008.127.
[10] E. Blanco, H. Shen, M. Ferrari, Principles of nanoparticle design for overcoming biological barriers to drug delivery, Nat. Biotechnol. 33 (2015) 941–951, https://doi.org/10.1038/nbt.3330.
[11] S.A. Dilliard, Q. Cheng, D.J. Siegwart, On the mechanism of tissue-specific mRNA delivery by selective organ targeting nanoparticles, Proc. Natl. Acad. Sci. 118 (2021) e2109256118, https://doi.org/10.1073/pnas.2109256118.
[12] Q. Cheng, T. Wei, L. Farbiak, L.T. Johnson, S.A. Dilliard, D.J. Siegwart, Selective organ targeting (SORT) nanoparticles for tissue-specific mRNA delivery and CRISPR–Cas gene editing, Nat. Nanotechnol. 15 (2020) 313–320, https://doi.org/10.1038/s41565-020-0669-6.
[13] S.T. LoPresti, M.L. Arral, N. Chaudhary, K.A. Whitehead, The replacement of helper lipids with charged alternatives in lipid nanoparticles facilitates targeted mRNA delivery to the spleen and lungs, J. Control. Release 345 (2022) 819–831, https://doi.org/10.1016/j.jconrel.2022.03.046.
[14] C.D. Sago, M.P. Lokugamage, F.Z. Islam, B.R. Krupczak, M. Sato, J.E. Dahlman, Nanoparticles that deliver RNA to bone marrow identified by in vivo directed evolution, J. Am. Chem. Soc. 140 (2018) 17095–17105, https://doi.org/10.1021/jacs.8b08976.

[15] K.L. Swingle, H.C. Safford, H.C. Geisler, A.G. Hamilton, A.S. Thatte, M. M. Billingsley, R.A. Joseph, K. Mrksich, M.S. Padilla, A.A. Ghalsasi, M.-G. Alameh, D. Weissman, M.J. Mitchell, Ionizable lipid nanoparticles for in vivo mRNA delivery to the placenta during pregnancy, J. Am. Chem. Soc. 145 (2023) 4691–4706, https://doi.org/10.1021/jacs.2c12893.
[16] H.C. Safford, K.L. Swingle, H.C. Geisler, A.G. Hamilton, A.S. Thatte, A.A. Ghalsasi, M.M. Billingsley, M.-G. Alameh, D. Weissman, M.J. Mitchell, Orthogonal Design of Experiments for Engineering of Lipid Nanoparticles for mRNA Delivery to the Placenta, Small. 2303568 (2023).
[17] R.E. Young, K.M. Nelson, S.I. Hofbauer, T. Vijayakumar, M.-G. Alameh, D. Weissman, C. Papachristou, J.P. Gleghorn, R.S. Riley, Lipid nanoparticle composition drives mRNA delivery to the, Placenta (2022), https://doi.org/10.1101/2022.12.22.521490.
[18] N. Chaudhary, A.N. Newby, M.L. Arral, S.S. Yerneni, S.T. LoPresti, R. Doerfler, D. M.S. Petersen, B. Fox, T. Coon, A. Malaney, Y. Sadovsky, K.A. Whitehead, Lipid nanoparticle structure and delivery route during pregnancy dictates mRNA potency, immunogenicity, and health in the mother and offspring, 2023, https://doi.org/10.1101/2023.02.15.528720, 2023.02.15.528720.
[19] H.C. Geisler, H.C. Safford, M.J. Mitchell, Rational Design of Nanomedicine for placental disorders: birthing a new era in Women's reproductive health, Small (2023) 2300852, https://doi.org/10.1002/smll.202300852.
[20] M.C. Frederiksen, Physiologic changes in pregnancy and their effect on drug disposition, Semin. Perinatol. 25 (2001) 120–123, https://doi.org/10.1053/sper.2001.24565.
[21] L. Ji, J. Brkić, M. Liu, G. Fu, C. Peng, Y.-L. Wang, Placental trophoblast cell differentiation: physiological regulation and pathological relevance to preeclampsia, Mol. Asp. Med. 34 (2013) 981–1023, https://doi.org/10.1016/j.mam.2012.12.008.
[22] M. Knöfler, S. Haider, L. Saleh, J. Pollheimer, T.K.J.B. Gamage, J. James, Human placenta and trophoblast development: key molecular mechanisms and model systems, Cell. Mol. Life Sci. 76 (2019) 3479–3496, https://doi.org/10.1007/s00018-019-03104-6.
[23] I. Brosens, P. Puttemans, G. Benagiano, Placental bed research: I. The placental bed: from spiral arteries remodeling to the great obstetrical syndromes, Am. J. Obstet. Gynecol. 221 (2019) 437–456, https://doi.org/10.1016/j.ajog.2019.05.044.
[24] C.G. Figueroa-Espada, S. Hofbauer, M.J. Mitchell, R.S. Riley, Exploiting the placenta for nanoparticle-mediated drug delivery during pregnancy, Adv. Drug Deliv. Rev. 160 (2020) 244–261, https://doi.org/10.1016/j.addr.2020.09.006.
[25] D.D. Smith, J.L. Pippen, A.A. Adesomo, K.M. Rood, M.B. Landon, M.M. Costantine, Exclusion of Pregnant Women from Clinical Trials during the Coronavirus Disease 2019 Pandemic: a review of international registries, Am. J. Perinatol. 37 (2020) 792–799, https://doi.org/10.1055/s-0040-1712103.
[26] K.M. Nelson, N. Irvin-Choy, M.K. Hoffman, J.P. Gleghorn, E.S. Day, Diseases and conditions that impact maternal and fetal health and the potential for nanomedicine therapies, Adv. Drug Deliv. Rev. 170 (2021) 425–438, https://doi.org/10.1016/j.addr.2020.09.013.
[27] K.L. Swingle, A.S. Ricciardi, W.H. Peranteau, M.J. Mitchell, Delivery technologies for women's health applications, Nat. Rev. Bioeng. 1 (2023) 408–425, https://doi.org/10.1038/s44222-023-00040-w.
[28] J. Tan, S. Shah, A. Thomas, H.D. Ou-Yang, Y. Liu, The influence of size, shape and vessel geometry on nanoparticle distribution, Microfluid. Nanofluid. 14 (2013) 77–87, https://doi.org/10.1007/s10404-012-1024-5.
[29] S.A. Dilliard, D.J. Siegwart, Passive, active and endogenous organ-targeted lipid and polymer nanoparticles for delivery of genetic drugs, Nat. Rev. Mater. 8 (2023) 282–300, https://doi.org/10.1038/s41578-022-00529-7.
[30] J.S. Refuerzo, F. Leonard, N. Bulayeva, D. Gorenstein, G. Chiossi, A. Ontiveros, M. Longo, B. Godin, Uterus-targeted liposomes for preterm labor management: studies in pregnant mice, Sci. Rep. 6 (2016) 34710, https://doi.org/10.1038/srep34710.
[31] J. Nong, P.M. Glassman, S. Reyes-Esteves, H.C. Descamps, V.V. Shuvaev, R. Y. Kiseleva, T.E. Papp, M.-G. Alameh, Y.K. Tam, B.L. Mui, S. Omo-Lamai, M. E. Zamora, T. Shuvaeva, E. Arguiri, C.A. Thaiss, J.W. Myerson, D. Weissman, S. E. Kasner, H. Parhiz, V.R. Muzykantov, J.S. Brenner, O.A. Marcos-Contreras, Targeting lipid nanoparticles to the blood brain barrier to ameliorate acute ischemic stroke, 2023, https://doi.org/10.1101/2023.06.12.544645, 2023.06.12.544645.
[32] N. Cureton, I. Korotkova, B. Baker, S. Greenwood, M. Wareing, V.R. Kotamraju, T. Teesalu, F. Cellesi, N. Tirelli, E. Ruoslahti, J.D. Aplin, L.K. Harris, Selective targeting of a novel vasodilator to the uterine vasculature to treat impaired Uteroplacental perfusion in pregnancy, Theranostics 7 (2017) 3715, https://doi.org/10.7150/thno.19678.
[33] J. Dong, Y. Cao, H. Shen, Q. Ma, S. Mao, S. Li, J. Sun, EGFR aptamer-conjugated liposome-polycation-DNA complex for targeted delivery of SATB1 small interfering RNA to choriocarcinoma cells, Biomed. Pharmacother. 107 (2018) 849–859, https://doi.org/10.1016/j.biopha.2018.08.042.
[34] B. Yu, H.C. Tai, W. Xue, L.J. Lee, R.J. Lee, Receptor-targeted nanocarriers for therapeutic delivery to cancer, Mol. Membr. Biol. 27 (2010) 286–298, https://doi.org/10.3109/09687688.2010.521200.
[35] R. Singh, M. Norret, M.J. House, Y. Galabura, M. Bradshaw, D. Ho, R.C. Woodward, T.G. St, I. Pierre, N.M. Luzinov, L.Y. Smith, K.S. Iyer Lim, Dose-dependent therapeutic distinction between active and passive targeting revealed using transferrin-coated PGMA nanoparticles, Small 12 (2016) 351–359, https://doi.org/10.1002/smll.201502730.
[36] D. Shi, S. Toyonaga, D.G. Anderson, *In vivo* RNA delivery to hematopoietic stem and progenitor cells *via* targeted lipid nanoparticles, Nano Lett. 23 (2023) 2938–2944, https://doi.org/10.1021/acs.nanolett.3c00304.
[37] L. Breda, T.E. Papp, M.P. Triebwasser, A. Yadegari, M.T. Fedorky, N. Tanaka, O. Abdulmalik, G. Pavani, Y. Wang, S.A. Grupp, S.T. Chou, H. Ni, B.L. Mui, Y. K. Tam, D. Weissman, S. Rivella, H. Parhiz, In vivo hematopoietic stem cell modification by mRNA delivery, Science 381 (2023) 436–443, https://doi.org/10.1126/science.ade6967.
[38] H. Parhiz, V.V. Shuvaev, N. Pardi, M. Khoshnejad, R.Y. Kiseleva, J.S. Brenner, T. Uhler, S. Tuyishime, B.L. Mui, Y.K. Tam, T.D. Madden, M.J. Hope, D. Weissman, V.R. Muzykantov, PECAM-1 directed re-targeting of exogenous mRNA providing two orders of magnitude enhancement of vascular delivery and expression in lungs independent of apolipoprotein E-mediated uptake, J. Control. Release 291 (2018) 106–115, https://doi.org/10.1016/j.jconrel.2018.10.015.
[39] L. Martínez-Jothar, S. Doulkeridou, R.M. Schiffelers, J. Sastre Torano, S. Oliveira, C.F. van Nostrum, W.E. Hennink, Insights into maleimide-thiol conjugation chemistry: conditions for efficient surface functionalization of nanoparticles for receptor targeting, J. Control. Release 282 (2018) 101–109, https://doi.org/10.1016/j.jconrel.2018.03.002.
[40] A.C. Marques, P.J. Costa, S. Velho, M.H. Amaral, Functionalizing nanoparticles with cancer-targeting antibodies: a comparison of strategies, J. Control. Release 320 (2020) 180–200, https://doi.org/10.1016/j.jconrel.2020.01.035.
[41] A. Beck, L. Goetsch, C. Dumontet, N. Corvaïa, Strategies and challenges for the next generation of antibody–drug conjugates, Nat. Rev. Drug Discov. 16 (2017) 315–337, https://doi.org/10.1038/nrd.2016.268.
[42] D. Rosenblum, A. Gutkin, R. Kedmi, S. Ramishetti, N. Veiga, A.M. Jacobi, M. S. Schubert, D. Friedmann-Morvinski, Z.R. Cohen, M.A. Behlke, J. Lieberman, D. Peer, CRISPR-Cas9 genome editing using targeted lipid nanoparticles for cancer therapy, science, Advances 6 (2020) eabc9450, https://doi.org/10.1126/sciadv.abc9450.
[43] N. Veiga, M. Goldsmith, Y. Granot, D. Rosenblum, N. Dammes, R. Kedmi, S. Ramishetti, D. Peer, Cell specific delivery of modified mRNA expressing therapeutic proteins to leukocytes, Nat. Commun. 9 (2018) 4493, https://doi.org/10.1038/s41467-018-06936-1.
[44] R. Kedmi, N. Veiga, S. Ramishetti, M. Goldsmith, D. Rosenblum, N. Dammes, I. Hazan-Halevy, L. Nahary, S. Leviatan-Ben-Arye, M. Harlev, M. Behlke, I. Benhar, J. Lieberman, D. Peer, A modular platform for targeted RNAi therapeutics, Nat. Nanotech. 13 (2018) 214–219, https://doi.org/10.1038/s41565-017-0043-5.
[45] L. Nuhn, E. Bolli, S. Massa, I. Vandenberghe, K. Movahedi, B. Devreese, J.A. Van Ginderachter, B.G. De Geest, Targeting Protumoral tumor-associated macrophages with Nanobody-functionalized Nanogels through strain promoted Azide alkyne cycloaddition ligation, Bioconjug. Chem. 29 (2018) 2394–2405, https://doi.org/10.1021/acs.bioconjchem.8b00319.
[46] R. Dudchak, M. Podolak, S. Holota, O. Szewczyk-Roszczenko, P. Roszczenko, A. Bielawska, R. Lesyk, K. Bielawski, Click chemistry in the synthesis of antibody-drug conjugates, Bioorg. Chem. 143 (2024) 106982, https://doi.org/10.1016/j.bioorg.2023.106982.
[47] M. Uhlén, L. Fagerberg, B.M. Hallström, C. Lindskog, P. Oksvold, A. Mardinoglu, Å. Sivertsson, C. Kampf, E. Sjöstedt, A. Asplund, I. Olsson, K. Edlund, E. Lundberg, S. Navani, C.A.-K. Szigyarto, J. Odeberg, D. Djureinovic, J.O. Takanen, S. Hober, T. Alm, P.-H. Edqvist, H. Berling, H. Tegel, J. Mulder, J. Rockberg, P. Nilsson, J. M. Schwenk, M. Hamsten, K. von Feilitzen, M. Forsberg, L. Persson, F. Johansson, M. Zwahlen, G. von Heijne, J. Nielsen, F. Pontén, Tissue-based map of the human proteome, Science 347 (2015) 1260419, https://doi.org/10.1126/science.1260419.
[48] L. Clemente, I.M. Bird, The epidermal growth factor receptor in healthy pregnancy and preeclampsia, J. Mol. Endocrinol. 70 (2023), https://doi.org/10.1530/JME-22-0105.
[49] L. Zhao, L. Sun, X. Zheng, J. Liu, R. Zheng, R. Yang, Y. Wang, In vitro fertilization and embryo transfer alter human placental function through trophoblasts in early pregnancy, Mol. Med. Rep. 21 (2020) 1897–1909, https://doi.org/10.3892/mmr.2020.10971.
[50] B. Marsh, R. Blelloch, Single nuclei RNA-seq of mouse placental labyrinth development, eLife 9 (2020) e60266, https://doi.org/10.7554/eLife.60266.
[51] R. Hastie, F.C. Brownfoot, N. Pritchard, N.J. Hannan, P. Cannon, V. Nguyen, K. Palmer, S. Beard, S. Tong, T.J. Kaitu'u-Lino, EGFR (epidermal growth factor receptor) signaling and the mitochondria regulate sFlt-1 (soluble FMS-like tyrosine Kinase-1) secretion, Hypertension 73 (2019) 659–670, https://doi.org/10.1161/HYPERTENSIONAHA.118.12300.
[52] D. Chen, K.T. Love, Y. Chen, A.A. Eltoukhy, C. Kastrup, G. Sahay, A. Jeon, Y. Dong, K.A. Whitehead, D.G. Anderson, Rapid discovery of potent siRNA-containing lipid nanoparticles enabled by controlled microfluidic formulation, J. Am. Chem. Soc. 134 (2012) 6948–6951, https://doi.org/10.1021/ja301621z.
[53] M.K. Greene, D.A. Richards, J.C.F. Nogueira, K. Campbell, P. Smyth, M. Fernández, C.J. Scott, V. Chudasama, Forming next-generation antibody–nanoparticle conjugates through the oriented installation of non-engineered antibody fragments, Chem. Sci. 9 (2018) 79–87, https://doi.org/10.1039/C7SC02747H.
[54] D.R. Elias, A. Poloukhtine, V. Popik, A. Tsourkas, Effect of ligand density, receptor density, and nanoparticle size on cell targeting, nanomedicine: nanotechnology, Biol. Med. 9 (2013) 194–201, https://doi.org/10.1016/j.nano.2012.05.015.
[55] B. Saha, T.H. Evers, M.W.J. Prins, How antibody surface coverage on nanoparticles determines the activity and kinetics of antigen capturing for biosensing, Anal. Chem. 86 (2014) 8158–8166, https://doi.org/10.1021/ac501536z.
[56] D. Yang, R. Kroe-Barrett, S. Singh, T. Laue, IgG charge: practical and biological implications, Antibodies (Basel) 8 (2019) 24, https://doi.org/10.3390/antib8010024.

[57] E. Drwal, A. Rak, E. Gregoraszczuk, Co-culture of JEG-3, BeWo and syncBeWo cell lines with adrenal H295R cell line: an alternative model for examining endocrine and metabolic properties of the fetoplacental unit, Cytotechnology 70 (2018) 285–297, https://doi.org/10.1007/s10616-017-0142-z.
[58] L. Woythe, P. Madhikar, N. Feiner-Gracia, C. Storm, L. Albertazzi, A single-molecule view at nanoparticle targeting selectivity: correlating ligand functionality and cell receptor density, ACS Nano 16 (2022) 3785–3796, https://doi.org/10.1021/acsnano.1c08277.
[59] Y.-P. Yang, H. Ma, A. Starchenko, W.J. Huh, W. Li, F.E. Hickman, Q. Zhang, J. L. Franklin, D.P. Mortlock, S. Fuhrmann, B.D. Carter, R.A. Ihrie, R.J. Coffey, A chimeric Egfr protein reporter mouse reveals Egfr localization and trafficking in vivo, Cell Rep. 19 (2017) 1257–1267, https://doi.org/10.1016/j.celrep.2017.04.048.
[60] J. Dackor, K.E. Strunk, M.M. Wehmeyer, D.W. Threadgill, Altered trophoblast proliferation is insufficient to account for placental dysfunction in Egfr null embryos, Placenta 28 (2007) 1211–1218, https://doi.org/10.1016/j.placenta.2007.07.005.
[61] M. Cataldi, C. Vigliotti, T. Mosca, M. Cammarota, D. Capone, Emerging role of the spleen in the pharmacokinetics of monoclonal antibodies, nanoparticles and exosomes, Int. J. Mol. Sci. 18 (2017) 1249, https://doi.org/10.3390/ijms18061249.
[62] I. Wojcik, D.E. Schmidt, L.A. de Neef, M.A.E. Rab, B. Meek, O. de Weerdt, M. Wuhrer, C.E. van der Schoot, J.J. Zwaginga, M. de Haas, D. Falck, G. Vidarsson, A functional spleen contributes to afucosylated IgG in humans, Sci. Rep. 11 (2021) 24045, https://doi.org/10.1038/s41598-021-03196-w.
[63] M.J. Eigenmann, L. Fronton, H.P. Grimm, M.B. Otteneder, B.-F. Krippendorff, Quantification of IgG monoclonal antibody clearance in tissues, mAbs 9 (2017) 1007–1015, https://doi.org/10.1080/19420862.2017.1337619.
[64] A.P. Weetman, Immunity, thyroid function and pregnancy: molecular mechanisms, Nat. Rev. Endocrinol. 6 (2010) 311–318, https://doi.org/10.1038/nrendo.2010.46.
[65] J. Dackor, M. Li, D.W. Threadgill, Placental overgrowth and fertility defects in mice with a hypermorphic allele of epidermal growth factor receptor, Mamm. Genome 20 (2009) 339–349, https://doi.org/10.1007/s00335-009-9189-2.
[66] K. Paunovska, C.D. Sago, C.M. Monaco, W.H. Hudson, M.G. Castro, T.G. Rudoltz, S. Kalathoor, D.A. Vanover, P.J. Santangelo, R. Ahmed, A.V. Bryksin, J.E. Dahlman, A direct comparison of in vitro and in vivo nucleic acid delivery mediated by hundreds of nanoparticles reveals a weak correlation, Nano Lett. 18 (2018) 2148–2157, https://doi.org/10.1021/acs.nanolett.8b00432.
[67] M.F. Attia, N. Anton, J. Wallyn, Z. Omran, T.F. Vandamme, An overview of active and passive targeting strategies to improve the nanocarriers efficiency to tumour sites, J. Pharm. Pharmacol. 71 (2019) 1185–1198, https://doi.org/10.1111/jphp.13098.
[68] N.D. Donahue, H. Acar, S. Wilhelm, Concepts of nanoparticle cellular uptake, intracellular trafficking, and kinetics in nanomedicine, Adv. Drug Deliv. Rev. 143 (2019) 68–96, https://doi.org/10.1016/j.addr.2019.04.008.
[69] M.J. Mitchell, M.M. Billingsley, R.M. Haley, M.E. Wechsler, N.A. Peppas, R. Langer, Engineering precision nanoparticles for drug delivery, Nat. Rev. Drug Discov. 20 (2021) 101–124, https://doi.org/10.1038/s41573-020-0090-8.
[70] M.A. Oberli, A.M. Reichmuth, J.R. Dorkin, M.J. Mitchell, O.S. Fenton, A. Jaklenec, D.G. Anderson, R. Langer, D. Blankschtein, Lipid nanoparticle assisted mRNA delivery for potent Cancer immunotherapy, Nano Lett. 17 (2017) 1326–1335, https://doi.org/10.1021/acs.nanolett.6b03329.
[71] K.J. Kauffman, F.F. Mir, S. Jhunjhunwala, J.C. Kaczmarek, J.E. Hurtado, J.H. Yang, M.J. Webber, P.S. Kowalski, M.W. Heartlein, F. DeRosa, D.G. Anderson, Efficacy and immunogenicity of unmodified and pseudouridine-modified mRNA delivered systemically with lipid nanoparticles in vivo, Biomaterials 109 (2016) 78–87, https://doi.org/10.1016/j.biomaterials.2016.09.006.
[72] K.A. Whitehead, J.R. Dorkin, A.J. Vegas, P.H. Chang, O. Veiseh, J. Matthews, O. S. Fenton, Y. Zhang, K.T. Olejnik, V. Yesilyurt, D. Chen, S. Barros, B. Klebanov, T. Novobrantseva, R. Langer, D.G. Anderson, Degradable lipid nanoparticles with predictable in vivo siRNA delivery activity, Nat. Commun. 5 (2014) 4277, https://doi.org/10.1038/ncomms5277.
[73] R. Repp, Th. Valerius, A. Sendler, M. Gramatzki, H. Iro, J.R. Kalden, E. Platzer, Neutrophils express the high affinity receptor for IgG (FcγRI, CD64) after in vivo application of recombinant human granulocyte Colony-stimulating factor, Blood 78 (1991) 885–889, https://doi.org/10.1182/blood.V78.4.885.885.
[74] R. Oostveen, A. Khera, S. Kathiresan, E. Stroes, K. Fitzgerald, M. Harms, B. Oakes, J. Kastelein, New approaches for targeting PCSK9: small-interfering ribonucleic acid and genome editing, Arterioscler. Thromb. Vasc. Biol. 43 (2023), https://doi.org/10.1161/ATVBAHA.122.317963.
[75] F. Yang, Q. Zheng, L. Jin, Dynamic function and composition changes of immune cells during Normal and pathological pregnancy at the maternal-fetal Interface, Front. Immunol. 10 (2019) 2317, https://doi.org/10.3389/fimmu.2019.02317.
[76] K.B. Johnsen, M. Bak, P.J. Kempen, F. Melander, A. Burkhart, M.S. Thomsen, M. S. Nielsen, T. Moos, T.L. Andresen, Antibody affinity and valency impact brain uptake of transferrin receptor-targeted gold nanoparticles, Theranostics 8 (2018) 3416–3436, https://doi.org/10.7150/thno.25228.
[77] R. Bazak, M. Houri, S. El Achy, S. Kamel, T. Refaat, Cancer active targeting by nanoparticles: a comprehensive review of literature, J. Cancer Res. Clin. Oncol. 141 (2015) 769–784, https://doi.org/10.1007/s00432-014-1767-3.
[78] N. Pardi, S. Tuyishime, H. Muramatsu, K. Kariko, B.L. Mui, Y.K. Tam, T.D. Madden, M.J. Hope, D. Weissman, Expression kinetics of nucleoside-modified mRNA delivered in lipid nanoparticles to mice by various routes, J. Control. Release 217 (2015) 345–351, https://doi.org/10.1016/j.jconrel.2015.08.007.